

Sputter Target Erosion and its Effects on
Long Duration DC Magnetron Sputter Coating

Michael Elliott Schoff

June 2009



UNIVERSITY OF CALIFORNIA, SAN DIEGO

Sputter Target Erosion and its Effects on Long Duration DC Magnetron Sputter
Coating

A thesis submitted in partial satisfaction of the requirements for the degree of Master
of Science

in

Engineering Sciences (Mechanical Engineering)

by

Michael Elliott Schoff

Committee in charge:

Professor Mark Tillack, Chair
Professor Farhat Beg
Professor George Tynan

2009

The Thesis of Michael Elliott Schoff is approved and it is acceptable in quality and form for publication on microfilm and electronically:

Chair

University of California, San Diego

2009

I dedicate this paper to my fiancée, Kimmy, whose love and support enable me to achieve what I never thought was possible.

TABLE OF CONTENTS

Signature Page	iii
Dedication	iv
Table of Contents	v
List of Figures	vi
Acknowledgements	viii
Abstract	ix
I. Introduction	1
II. Sputter Coating Fundamentals	4
III. Beryllium Sputter Coater	13
IV. Copper Coater Automation and Experimental Setup	16
V. Preliminary Observations	21
VI. Related Copper Run Data	24
VII. Coating Rate vs. Power	26
VIII. Characterizing the Life of Sputter Targets	29
7.1 Introduction	29
7.2 Sputter Gun Power Supply	29
7.3 Copper Sputter Target	30
7.4 Silicon Substrate	37
7.5 Quartz Crystal Microbalance	39
7.6 Summary of Results	40
IX. Conclusion	44
Appendix	47
References	54

LIST OF FIGURES

Figure 2.1: Sputter yields for argon incident on copper and beryllium at normal incidence	5
Figure 2.2: Normalized sputter yield for argon incident on copper as a function of incident angle ³	6
Figure 2.3: Diagram of sputter coater	7
Figure 2.4: Extrapolated magnetic field lines from measured magnetic field ⁸	8
Figure 2.5: Copper sputter target with race track	9
Figure 2.6: Diagram of cosine dependence	11
Figure 3.1: Beryllium gun currents and voltages vs time, at ~25Watt power output ..	14
Figure 4.1: Silicon substrate with cross pattern	16
Figure 4.2: Inside of coating chamber	17
Figure 4.3: Test chamber shown from above	18
Figure 4.4: Test chamber shown from the door	18
Figure 5.1: Comparison of sputter plasma for new and used Al targets.....	21
Figure 6.1: A collection of voltage and current evolutions in time from five consecutive coatings on the copper sputter gun.....	24
Figure 6.2: A collection of coating rates in time measured by a QCM from five consecutive coatings on the copper sputter gun.....	25
Figure 7.1: Equivalent sputter yield compared to the empirical sputter yield	27
Figure 7.2: Coating rate as a function of gun power set point.....	28
Figure 8.1: Gun power supply data as a function of coating time	30
Figure 8.2: Rate of mass sputtered from target as a function of time.....	31
Figure 8.3: Comparison between calculated yield from sputtered mass and empirical copper sputter yield curve.....	32

Figure 8.4: Measured depth profile of copper target after each run	34
Figure 8.5: Depth profile of copper target as function of the radius	34
Figure 8.6: Normalized radial race track profiles	35
Figure 8.7: Magnetic field lines near the target	35
Figure 8.8: Comparison of the copper sputter target for different lengths of coating time	36
Figure 8.9: Copper thickness on silicon substrate from both axes	38
Figure 8.10: Thickness on silicon substrate with \cos^4 fit	39
Figure 8.11: Copper coating rate as measured by the QCM.....	40
Figure 8.12: Comparison of QCM equivalent and empirical sputter yields	41
Figure 8.13: Normalized coating rates.....	42
Figure 8.14: Diagram of focusing effect of race track on sputtered material	42
Figure 10.1: Adjust Coater Settings subvi front panel.....	47
Figure 10.2: Adjust Coater Settings subvi block diagram.....	48
Figure 10.3: Be Coater Main vi front panel.....	49
Figure 10.4: Data Recorder subvi front panel.....	50
Figure 10.5: Data Recorder subvi block diagram	51
Figure 10.6: Multiple Coater Datalog vi front panel	52
Figure 10.7: Multiple Coater Datalog vi block diagram.....	53

ACKNOWLEDGMENTS

I would like to thank Mark Tillack from UCSD, who advised me and pushed me to search deeper for the underlying meaning and understanding. I would like to thank Haibo Huang for his physical insight and guidance throughout my time at General Atomics. I would also like to acknowledge Sam Eddinger, Hongwei Xu, Javier Vasquez, Tim Fuller, Abbas Nikroo, Wen Wu, and Paul Parks, from General Atomics who assisted me in the technical and theoretical aspects of this paper.

ABSTRACT OF THE THESIS

Sputter Target Erosion and its Effects on Long Duration DC Magnetron Sputter
Coating

by

Michael Elliott Schoff

Master of Science in Engineering Sciences (Mechanical Engineering)

University of California, San Diego, 2009

Professor Mark Tillack, Chair

Plasma discharge sputter coaters have been used to create uniform thin layers of practically any target material. For Inertial Confinement Fusion research, a batch of several 1-2 mm diameter inertial fusion target shells are grown using several sputter coaters that run for 2-3 weeks and use 2-3 targets per gun. As the targets are consumed, a well documented ring or “race track” indentation develops on the target surface. The changing geometry of the target has been shown to affect the operating

parameters of the sputter gun, as well as the quality of the deposition. Current methods do not achieve the quality and reproducibility that specifications demand. The purpose of this thesis is to characterize the sputtering process as it evolves through the life of a target, to better understand the sputtering process and ultimately to provide the means to produce higher quality, reproducible shells. Several production sputter coaters were automated to provide enhanced control and process data as a function of time. An experiment was then conducted that documented the deposition from an unused copper target through 90% of its initial thickness in three separate runs. It was found that the sputter yield matches with the empirical calculation, and is determined by the cathode voltage. The distribution of coated material for small θ retains the cosine to the fourth power dependence, even as the sputter yield decreases with increasing target erosion. As the target erodes, the sputtered material is focused around small θ because of changing target geometry and resputtering.

I. INTRODUCTION

One of the research directions in the quest for nuclear fusion of hydrogen as an energy source strives for ignition through inertially confined heavy hydrogen fuel pellets. When shot with specialized high-power lasers, the outer shell ablates and compresses the fuel. To achieve uniform and complete utilization of the hydrogen fuel, the approximately two millimeter diameter spherical shells that contain the fuel and supply the inertia have very strict requirements for composition, size, shape, sphericity, surface roughness, total density and radial density profiles, layer thickness and permeation. To achieve the desired quality, the shells are grown on spherical molds with the use of sputter coaters.

Sputter coaters are very useful in depositing very thin layers of almost any material and are very common in industry, such as microelectronics fabrication. For typical applications, sputter coaters are used for minutes or hours at most. When used for the growth of shells for Inertial Confinement Fusion (ICF), the sputtering process for typical shells takes approximately two to three weeks of constant sputtering and involves two to three different targets for each of the three sputter guns. During the life of the sputter target, which lasts about a week, the target erodes non-uniformly and the coating process parameters, such as the cathode voltage do not remain constant. Small changes in the sputtering process can be compounded into undesirable fluctuations in shell quality. Even a gentle trend will have negative effects that become apparent when the fully utilized targets are replaced by new targets to complete the coating. For example, the argon incorporation at the substrate, resulting

from incident argon ions burrowing in the outer shell layers, shows a decreasing trend for each target, but the interface between targets is sharp and above tolerable atomic percent composition. Sputter coating has been a popular subject of research for more than 100 years; however, since most applications last only short durations, little research has been done on characterizing the sputter coating during the lifetime of a sputter target and comparing coatings with targets at different levels of erosion. For our application of sputtering, this time dependent variation in sputter coating is crucial to understand, so that we can produce a high volume of higher quality shells that meet stringent specifications.

In an effort to understand the time-evolution of the sputtering process and to improve the quality of sputter coated shells, I automated several sputter coating chambers to provide enhanced control and data collection. I also carried out an experiment to characterize the time variations of the target, the coating on the substrate, and the process in general. From this data, the time evolution of the sputtering process and its effects on the deposition of material are analyzed.

The next section describes sputter coating in general and the specific apparatus used in my experiments. The automation of and data from the beryllium coater that produces inertial fusion target shells is discussed in Section III. In Section IV, I present the experimental setup and automation of the copper coater. After some preliminary, qualitative observations about the changing target and coating, I will discuss the relationship of coating rate with sputter gun power output. In Section VII, I will display the data from the experiment spanning the life of a copper target. Here

the changing process will be measured at the sputter source (target) and destination (substrate, QCM). From these data, a better understanding of the effect of target erosion on the sputter coating process can be achieved. Also, screen dumps and descriptions of the developed automation programs can be found in the Appendix.

II. SPUTTER COATING FUNDAMENTALS

Deposition of material from plasma discharge sputter coating results from the interaction of positively ionized atoms from a background gas that are accelerated towards a negatively charged target (cathode). This process is a type of physical vapor deposition (PVD). The background gas is typically an inert gas that will more easily ionize and does not easily react chemically, like argon, while target can be virtually any material, though special techniques must be used if sputtering an insulator, such as using a time varying cathode potential. The energetic particles bombard the surface of the target and cause a cascade of collisions that transfer the impact energy within the target, resulting in the occasional ejection of one or more atoms of the target material. To quantify the ejection, a sputtering yield is defined as the average number of atoms removed from the target per incident particle. Theoretical sputter yields are derived from collision theory, where sputtering is viewed approximately as a collision of a hard sphere with another sphere or group of spheres. In each collision, momentum and energy must be conserved. Each incident particle creates a cascade of collisions in various directions, dispersing the energy and momentum. Because these collisions are not limited to one dimension, the transfer of energy and momentum can be redirected toward the surface and, if there is enough energy, target material can be kicked off the target. In addition to sputtered target material, the impacts of the high energy ions eject secondary electrons that are repelled from the negatively charged cathode and create ions from interactions with the neutral background gas.

Sputter yields vary for incident particle and charge, target material, incident angle and cathode (target) potential. In Figure 2.1, the sputter yields for argon incident on copper and beryllium are displayed at normal incidence¹. Buried within these curves is the added dependence of the sputtering yield on the nuclear stopping cross section that determines the penetration distance of the incident energetic ions and the threshold energy, the minimum energy the target atoms must have in order to escape the target². The normalized sputter yield for argon incident on copper as a function of the incident angle³ is shown in Figure 2.2. From the point of view of a cascade of collisions, an incident angle of about 45° would result in a higher sputter yield because the component of momentum into the target would be smaller, though the total momentum and energy would remain the same. The transfer of momentum and energy would stay closer to the surface and leave a higher probability of material

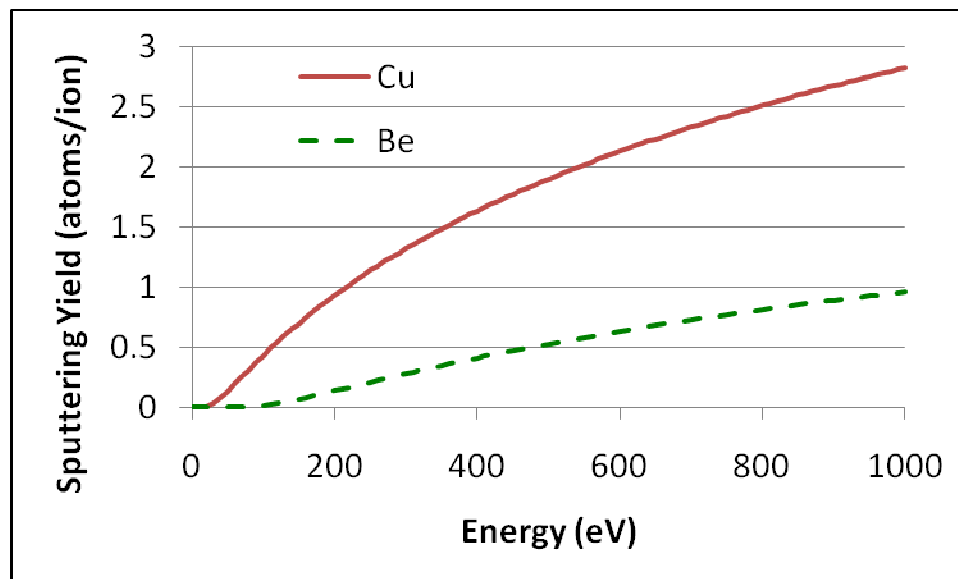


Figure 2.1: Sputter yields for argon incident on copper and beryllium at normal incidence

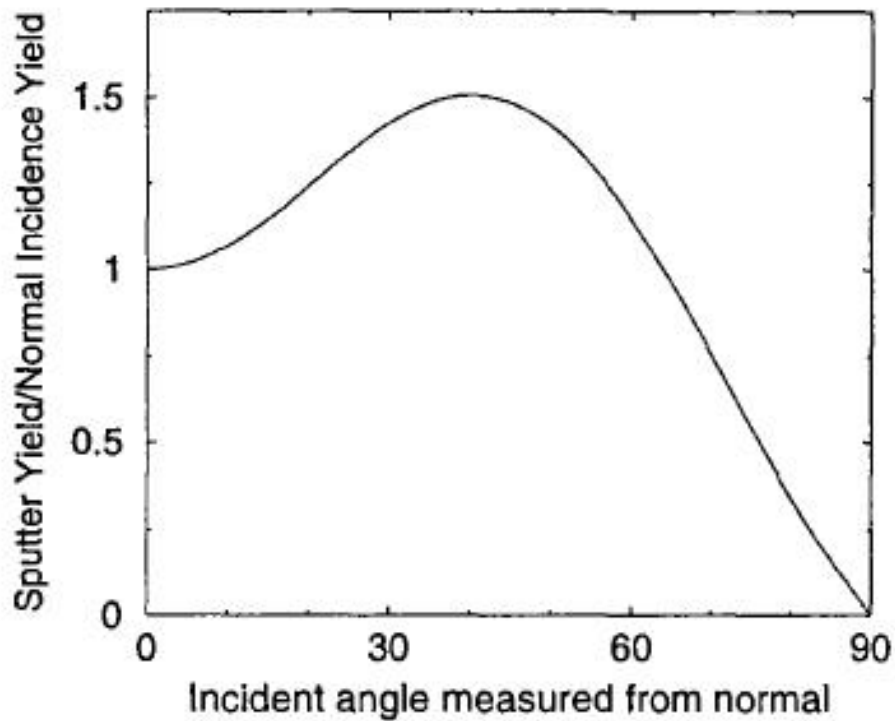


Figure 2.2: Normalized sputter yield for argon incident on copper as a function of incident angle³

being sputtered. If we were to increase the angle further to 90°, the incident particle would barely graze the surface and most likely bounce off the surface and not transfer all of its energy. This would account for the drop off in sputter yield as the angle approaches 90°.

The evacuated coating chamber is backfilled with argon gas to pressures around 5 mTorr. The argon gas becomes ionized from interactions with free energetic electrons, leading to the creation of dilute neutral plasma (approximately equal numbers of electrons and ion charges). Most of the ions in the plasma do not interact with the cathode due to electron shielding within the plasma, but those closest to the cathode (less than 1mm away) are attracted and accelerated across the potential

sheath⁴⁻⁶. The ions that are created in the sheath are accelerated toward the cathode and intersect the plane of the target in the normal direction. For cathode potentials on the order of 100V or more, the thermal energy is much smaller than the electrical energy, and therefore the argon atoms in the sheath, once ionized, travel in straight lines from their point of ionization to the cathode. Because the sputtering occurs very close to the point of impact, the majority of sputtering on the target will occur where the majority of ions are created and distributed⁷.

There are many types of sputter coaters, utilizing various designs for different applications. My data involve DC magnetron sputter coaters that incorporate a direct current (DC) potential bias on the cathode and a static closed-loop magnetic field. The magnetic field consists of a central magnet (North) and an outer ring magnet (South) directly behind the target, as in Figure 2.3. The resulting field lines have been

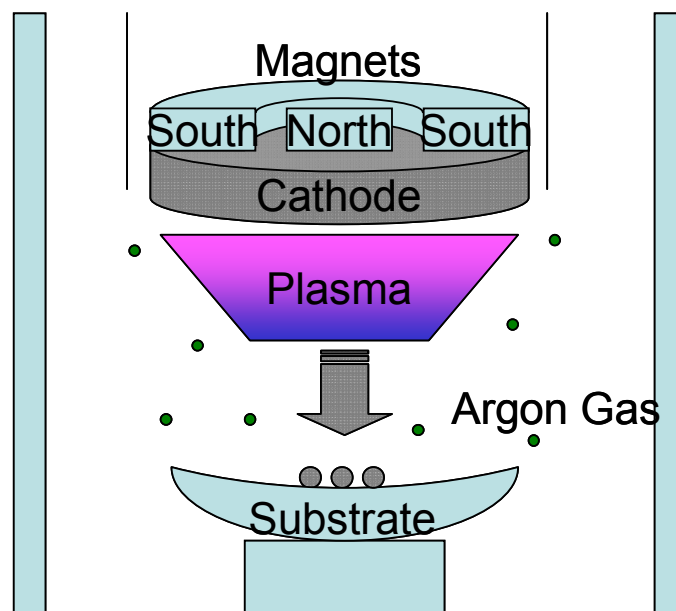


Figure 2.3: Diagram of sputter coater

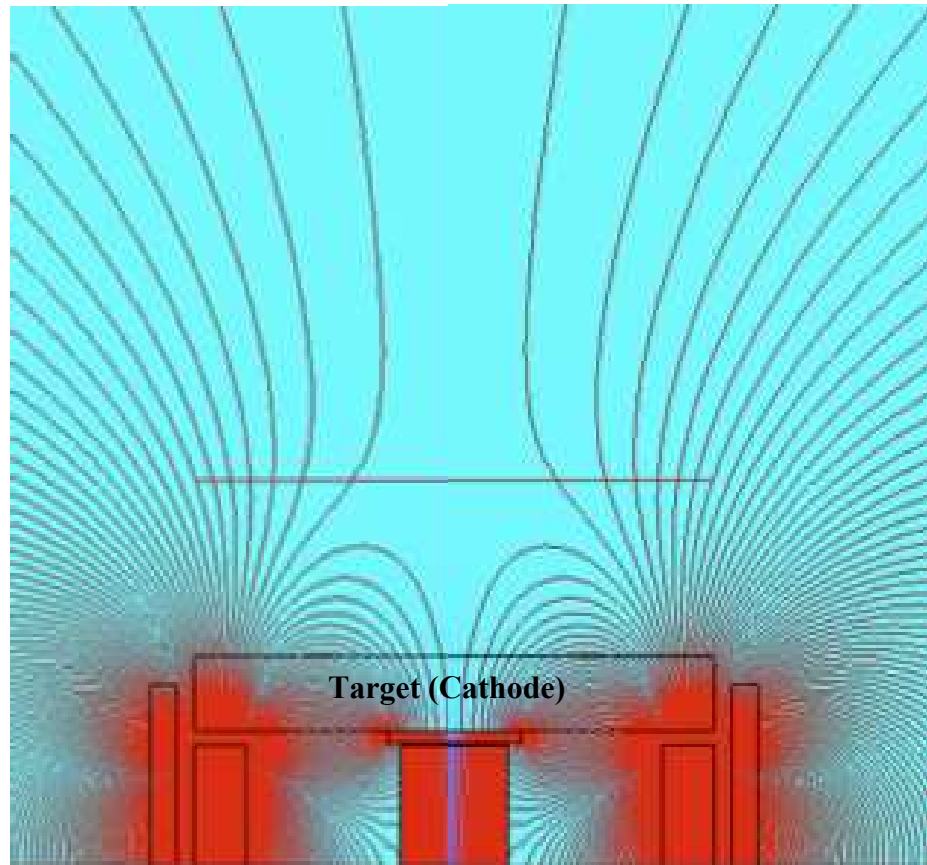


Figure 2.4: Extrapolated magnetic field lines from measured magnetic field⁸

measured using a Langmuir probe and the extrapolation⁸ is plotted to scale with the gun and target in Figure 2.4. This configuration traps free electrons along the magnetic field lines close to the target, so that the ionization of the background gas occurs closer to the target than if there was no magnetic field. This allows the background pressure to be much lower, while still maintaining high ionization and sputtering⁹⁻¹⁰. Also, with a lower pressure, the mean free path of sputtered atoms from the target is much greater, allowing more target material to reach the substrate with fewer collisions with other particles in the chamber.

As copper is sputtered off the target, it must travel through the plasma in order to reach the substrate. Through numerical analysis, it has been shown that the argon ion density follows that of the electron density, but the copper ion density is approximately two orders of magnitude lower than the argon ion density¹¹. The copper ion, which is positive like the argon ion, would be attracted to the cathode and would cause more sputtering, or self-sputtering (incident and target particle are the same material). This effect, however, is very small and calculated to be negligible¹¹. For other materials, like beryllium, the self-sputtering could be very important¹².

The combination of the confinement of electrons along the magnetic field lines and the negative electric potential on the cathode provides the highest probability of electrons being located where the magnetic field lines are parallel to the plane of the initial target surface, which corresponds to a potential well. As a result, the majority of collisions between argon atoms and free electrons and thus ions created are located here, at about half of the target radius. The distribution of ions and therefore the



Figure 2.5: Copper sputter target with race track

majority of sputtering are concentrated at this radius¹³⁻¹⁴. The spatially dependent erosion develops a ring or “race track” devoid of target material, as shown in Figure 2.5. The shape of the erosion pattern is dependent on the strength of the cathode voltage and magnetic field. An increase in magnetic field strength will make the race track narrower, while an increase in cathode voltage will broaden the race track¹⁵⁻¹⁶. Once the depth of the race track approaches the thickness of the target, the target can no longer be used without risking damage to the gun or introducing contaminants into the coating. This erosion pattern restricts the use of sputter targets to only a fraction of the initial mass.

The distribution of sputtered material on the substrate has also been investigated experimentally and numerically¹⁷⁻²². The distribution is largely dependent on the magnetic field strength and configuration, and since magnetic fields vary for each coater, there is no absolute rule. The source of sputtering is also very complicated as it is non-uniform and depends on the ion distribution. It is agreed, however, that if we treat the sputter source as a point source, the initial distribution of sputtered material from the sputter target is proportional to the cosine of the angle from the surface normal. Once sputtered, the amount of material collected at the substrate is predominately a function of the geometry. To a good approximation (when the angle θ is small) the distribution is proportional to the cosine of θ to the fourth power. A diagram of this dependence is shown in Figure 2.6. The first cosine dependence results from the initial sputtering of a point source. Superimposing arcs over the radius, the intensity decreases like $1/r^2$, which is related to the cosine squared

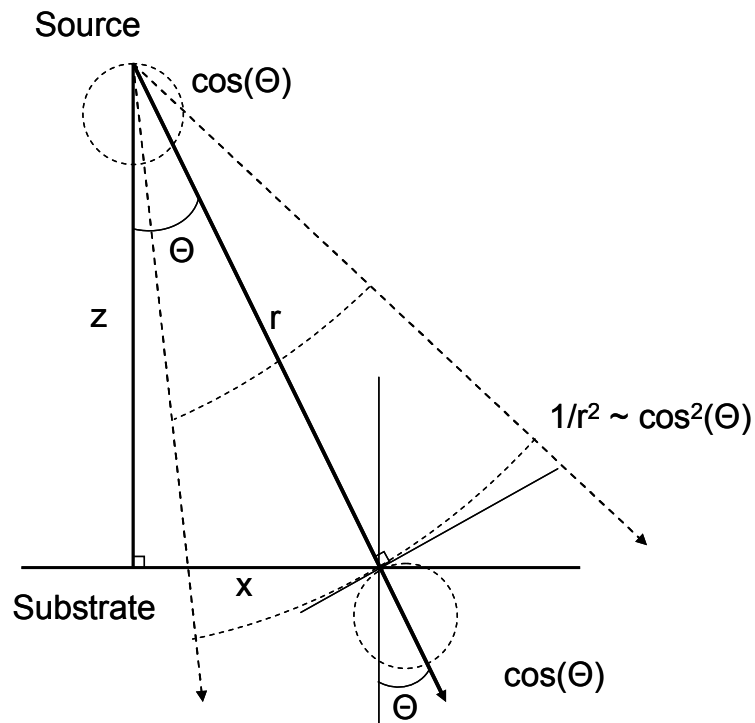


Figure 2.6: Diagram of cosine dependence

at constant height z . The last cosine dependence results from the incident material not being normal to the surface and so the projection on the surface reduces the deposition by another factor of cosine. Multiplying these factors together, we are left with a deposition distribution proportional to the cosine of θ to the fourth power.

The sputter source is not a point source, however, so the cosine to the fourth power distribution is not completely accurate. Two point sources would tend to be more flat in the region between them, and so a symmetrically distributed ring of sources with finite width would tend to deposit a flatter distribution on the substrate. Some have found the exponent of the cosine to be as little as 2.7, while others have used a similar geometric equation that does not include the cosine function. The difference between the latter and the cosine to the fourth power is less than 1% at a

radius of 2 inches and a height of 7.25 inches. Note that this difference is more prominent when the height is decreased or the aspect ratio is closer to unity.

Though many experiments and models have characterized the sputter coating process very well for short time periods, little is known about the process for very long coating runs that last the lifetime of the target. Understanding the changing behavior of the coating process over an extended period of time is crucial to improving the quality and reproducibility of inertial fusion shells. Most numerical models can simulate the electron and ion distributions above a new target, but it is much more difficult to resolve the complex geometry of the boundary conditions of an eroded or eroding target. Because of this changing geometry, the physics of erosion, redeposition, release of particles, and the transport of material evolve. In this work, experiments were performed to characterize the target erosion and substrate deposition throughout the life of a target. By replicating identical data collection at different stages of target erosion, I was able to reveal the erosion dependent variations. I also automated several coaters to assist in process control, monitoring, and data recording during the actual coating. From these data, possible explanations for the changes in erosion and deposition were explored.

III. BERYLLIUM COATER AUTOMATION

To determine how the sputter coating process changes throughout the weeklong coating process, the first step was to automate and record data on the production coaters. Previously, little data was recorded by hand at most once a day. Any automated data recording would be a significant improvement, but for the best results, full automation was needed. With that in mind, I wired and connected all of the various devices and components used to run the sputter coater. I incorporated analog and digital input and output signals, along with RS-232 serial communication protocols. I then created a LabVIEW program to connect and integrate the various components, including several sputter gun power supplies, background gas pressure transducer and controllers, valves, switches, and substrate bias power supply. For images and diagrams of the program, please look in the Appendix. This automation allowed for a more precise control of system parameters than the operator could achieve manually.

Inertial fusion shells contain several layers of varying copper dopant in beryllium. This is achieved by using three beryllium sputter guns and one copper sputter gun, and varying the power. Instead of manually varying the copper power output, which needed to be done at a specific time, the automated program could accurately change the power at any preset time. Also, the program was able to create any variation or combination of layers that would have been impossible to do manually. A profile could also be stored and reused for increased repeatability.

In addition, the program could monitor and record the system parameters, providing invaluable data that could not be provided by a human operator, especially as the process spans several weeks. When the operator left work at the end of the day or for the weekend, the program would continue to monitor the process and record data, an invaluable tool for such a long unsupervised process. The data is continuously read and averaged to provide data with the least noise and interference.

The process could also be accurately terminated, even when the operator was not present or after working hours. This feature adds efficiency, accuracy and repeatability as the program could terminate the process at a preset time. Automatically updating graphs would display all data previously collected and provide real-time status of the current process. Should there be any errant behavior during the

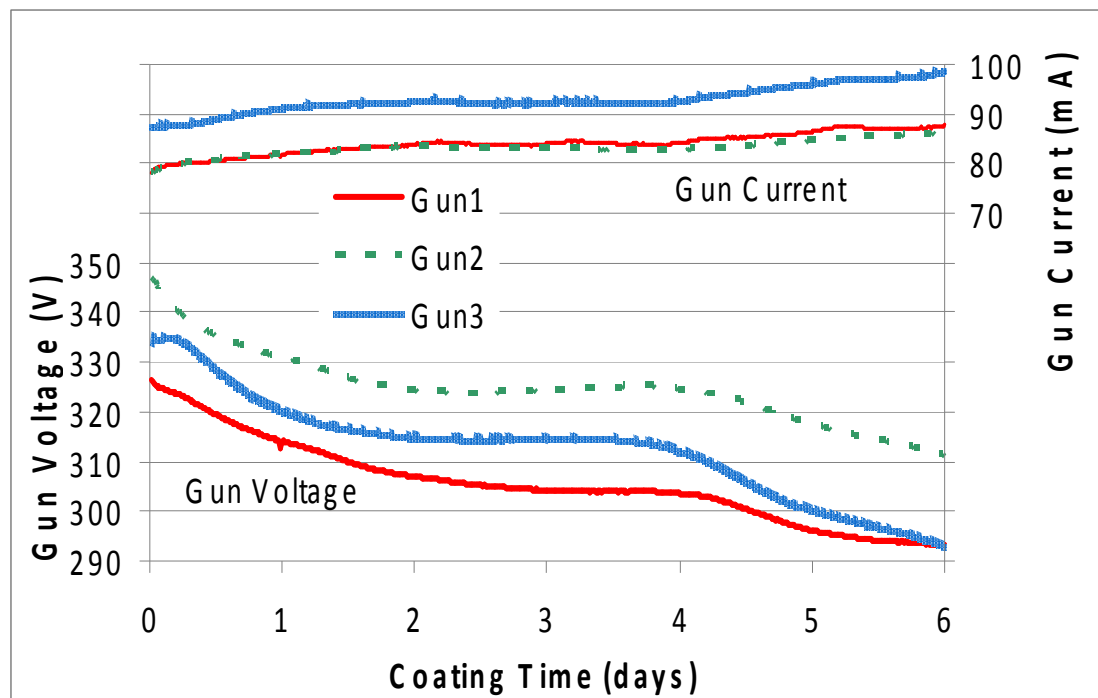


Figure 3.1: Beryllium gun currents and voltages vs time, at ~25Watt power output

run that would render a batch of shells useless (power supply failure, drastic changes in pressure, etc.), the coating run would be terminated right away, saving time and money by not wasting time coating on shells that will not be used. The quality of the shells could also be compared to the process data, correlating measured defects with run data.

A sample of run data is shown in Figure 3.1. It was previously known that the voltage decreases and the current increases in time as the target erodes, but not with the current resolution. Though this data was very interesting, it did not provide enough information to determine how the entire coating process changes as the target erodes. This process has many overlapping variables and complexity, such that a matrix of all possible settings would not be sufficient for understanding of the process. In addition, the toxicity of the beryllium target restricted my access and ability to collect additional data on the target or substrate. A simpler, more accessible experiment was needed to collect new and enlightening data.

IV. COPPER COATER AUTOMATION AND EXPERIMENTAL SETUP

To gain more information and understanding of the time varying coating process, I automated three more coaters and designed a simplified experiment using a single sputter gun with a copper target. Copper is a suitable substitute because it is safe, conducting, cheap, readily available, prevalent in literature and conducive to sputtering with beryllium.

For my experiment, I measured the effect of the changing target by measuring the deposition of copper. Directly beneath the target on a secured aluminum block, I placed a four inch diameter silicon wafer with two thin pieces of vacuum approved tape placed perpendicularly, as is shown in Figure 4.1. The copper would be coated directly on the silicon wafer that was the substrate for the experiment. Next to the silicon wafer, I mounted a Quartz Crystal Microbalance (QCM) that measures the amount of material that has been sputtered at that location. The QCM is secured and angled toward the gun. An actual picture of the inside of the chamber is shown in

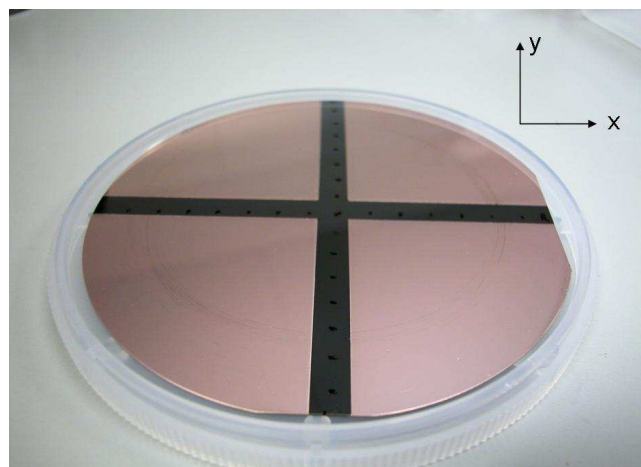


Figure 4.1: Silicon substrate with cross pattern



Figure 4.2: Inside of coating chamber

Figure 4.2, with the dimensions and layout of the test chamber shown from above in Figure 4.3 and from the front in Figure 4.4.

Using this coating chamber with a simpler design, easier access and safe target, I was able to more easily monitor the variations in time of the coating process. Before each coating run, a new silicon wafer and QCM crystal were installed. Also, I

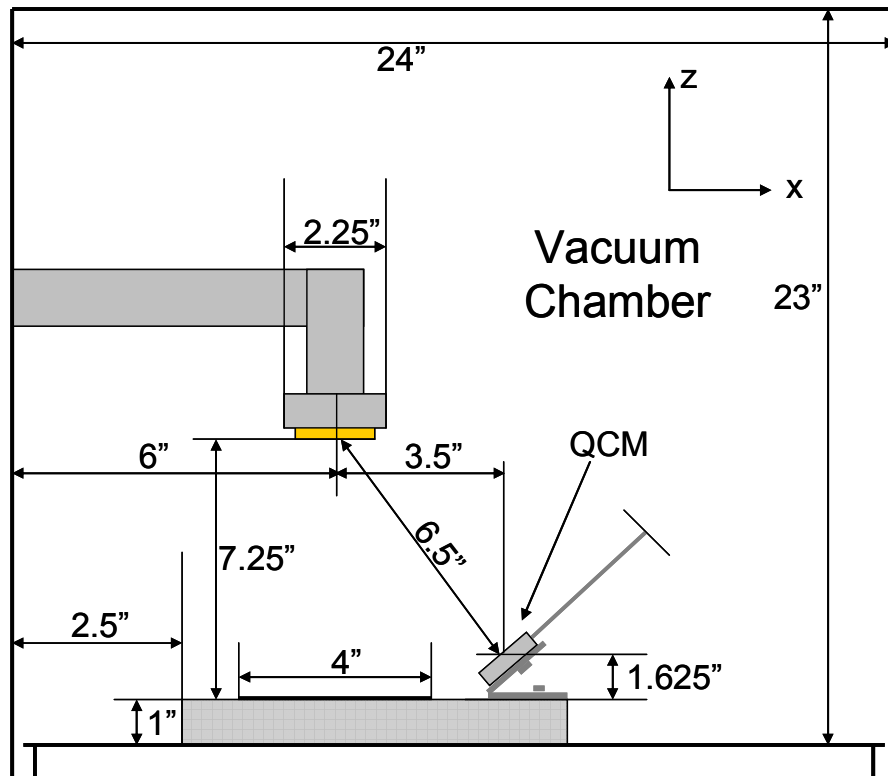


Figure 4.3: Test chamber shown from above

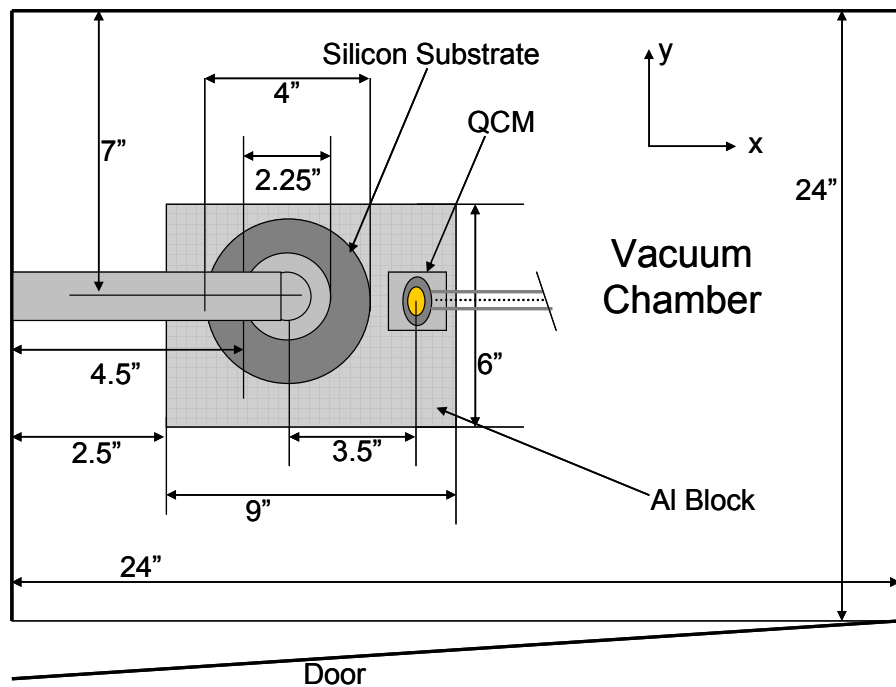


Figure 4.4: Test chamber shown from the door

weighed the target to determine its mass and calculated the thickness as a function of position on the target with a measuring microscope. Even though the race track profile is axially symmetric, a scratch placed on the backside of the target allowed me to reinsert the target in the same direction each time. The tape on the silicon wafers that were coated with copper was carefully removed, leaving a cross where no copper had been deposited. I marked a grid spaced every quarter of an inch on each axis (see Figure 4.1). At each point on both axes, I recorded the coated thickness using a stylus probe. From these data I was able to obtain the distribution of coated material as a function of the position on the silicon substrate.

With the automation and data logging, I was able to record the power supply characteristics of the sputter gun output (voltage, current and power) and the chamber pressure from analog voltage signals read through a National Instruments Data Acquisition Board. These signals were read ten thousand times per second and then averaged for improved accuracy and reduced noise. The signals were also transmitted in shielded twisted cabling to dampen electrical noise and interference. The QCM was interfaced through the serial port providing digital communication and data collection. Data collected from the QCM includes the thickness of material coated on the crystal and a time averaged rate of deposition. All of this data was recorded with the time once a second, during the entire experiment. See Appendix for pictures and diagrams of the automation and data logging program.

My experiment was divided into three separate coating runs using the same target. The first run started with a brand new target and lasted 16 hours. The second

and third runs lasted 13 and 8 hours, respectively. The runs were completed in three consecutive days. The sputter guns were set to operate in constant power mode, at a set point of 100 Watts, allowing the voltage and current to be determined by the system. The chamber pressure was likewise set to remain constant at 5 mTorr.

V. PRELIMINARY OBSERVATIONS

Before diving into the experimental data, I would like to discuss some of the qualitative descriptions of the target and the coating process that indicate it is not constant in time. Many production coatings have been measured to contain time-dependent variations in several characteristics of shells, the cause of which has not yet been determined. Though the operating conditions (sputter gun power set point, argon background gas pressure, internal geometry of coater, etc.) were fixed for the entire run, the variations in time are apparent.

From a preliminary experiment conducted by Haibo Huang and myself, the

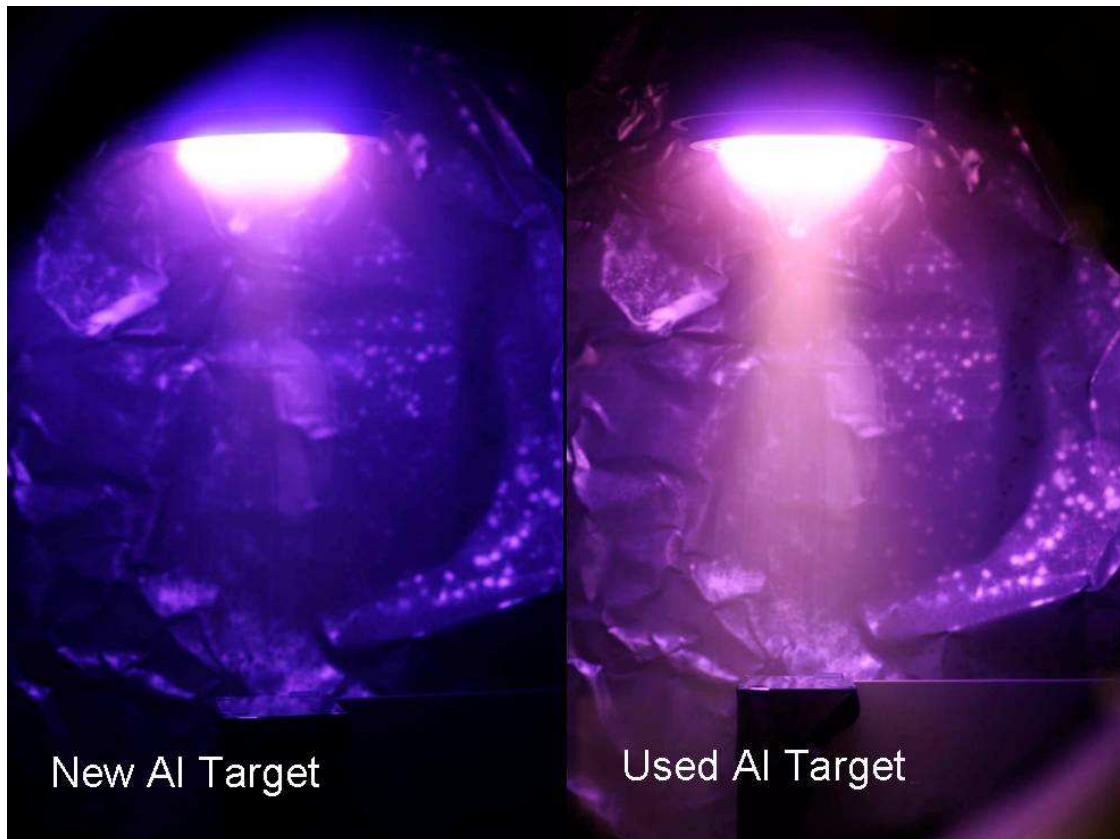


Figure 5.1: Comparison of sputter plasma for new and used Al targets

plasma was photographed for various operating conditions. The two images in Figure 5.1 consist of the same coater and operating conditions, except that the target on the left was new, while the target on the right was heavily eroded (~75%). From these two images, differences in the color, intensity and shape of the plasma regions are evident. Though there is quantitative data involved in these images, I provide them merely as an indication of a changing process in time.

Another indication of variability resides with the target itself. The erosion is not uniform across the planar surface of the target, but is instead concentrated in a circular ring or “race track” corresponding to the location of highest ion density. As the target erodes, the surface is no longer a flat plane, but instead contains a circular valley, whose surface is now not necessarily normal to the incident ions. The sputter yield has been documented to have a strong angular dependence, thus greatly changing the dynamics of the process. To complicate matters further, the structure of the potential sheath is also altered by the changing geometry of the target, the proximity of the plasma to the target as it feels the stronger magnetic field closer to the magnets, and the plasma itself. I do not intend to delve into the complexities of the plasma-target interactions for various stages of target erosion, though a future topic of interest might be to simulate the erosion of the target with an initial race track by defining the ion density and calculating the effect of the altered geometry on the erosion profile of the target, magnetic field, and potential sheath. For this paper, however, I again make this observation just to illustrate that the process is not constant in time and that I will

be focusing on the effects of this time variation, however small, and not on the causes.

It is in this manner that I will attempt to shed some light on this complex problem.

VI. RELATED COPPER RUN DATA

Once the automation was complete, the three metal coaters were first used for production coatings. Various metals such as copper, aluminum, gold and boron are coated on many types of inertial fusion parts components. Using the data log and automation program, the thickness and gun power supply info were being monitored and recorded during the run. Data from five consecutive runs with the same sputter target, each run lasting about an hour, are plotted in Figure 6.1. The sputter gun voltage and current are plotted against the amount of time the copper sputter target was used. Though the copper target was run at 100 Watts, this graph shows similar trends as the beryllium data run at 25 Watts, shown in Figure 3.1. These two sets of data indicate a time evolution of the gun power supply characteristics that is independent of target material, sputter gun, or gun output power set point. This data

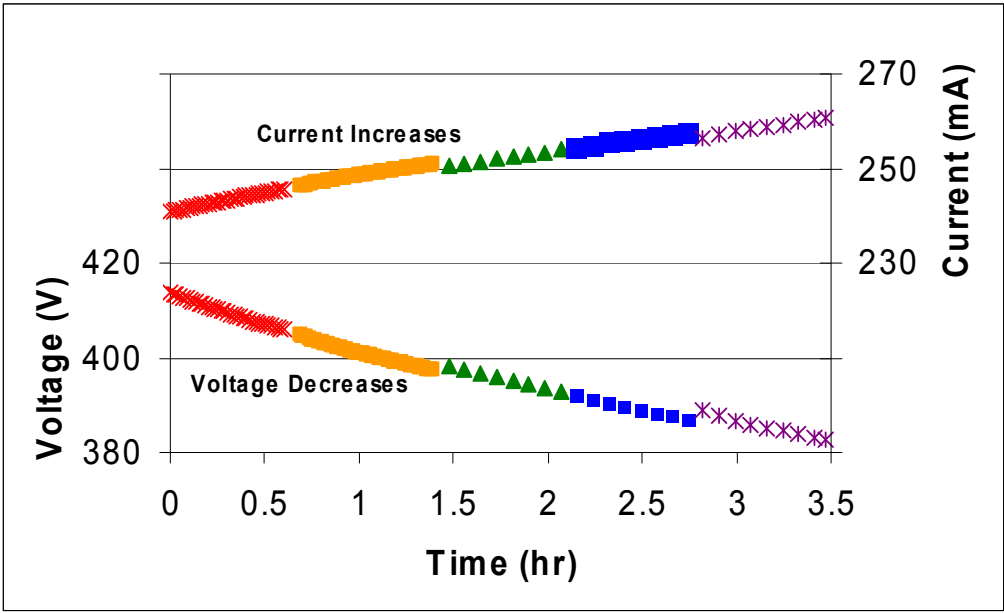


Figure 6.1: A collection of voltage and current evolutions in time from five consecutive coatings on the copper sputter gun

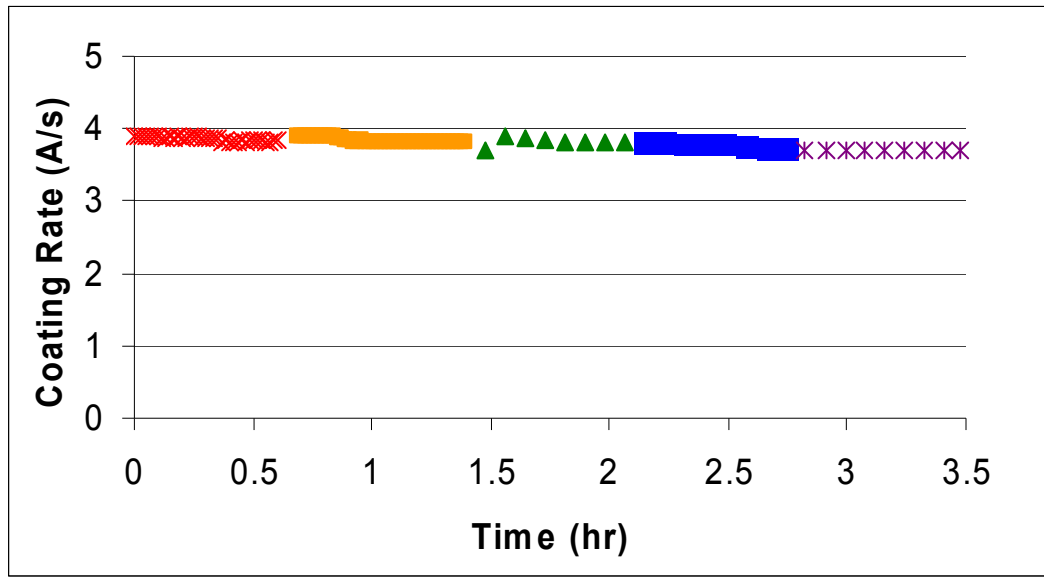


Figure 6.2: A collection of coating rates in time measured by a QCM from five consecutive coatings on the copper sputter gun

would indicate that the erosion of the target has an effect on the coating and the gun power supply characteristics. This also shows the difference in time scales, where the change in characteristics for each short run is not very large, but between runs with a new target and an almost fully eroded target the difference can be much greater, as will be shown in later experiments.

The coating rate data, as measured by a QCM, for the same five runs is plotted in Figure 6.2. A slight downward trend is noticeable, similar to the voltage decreasing in time. This behavior can be explained simply by looking at the plot of the sputtering yield as a function of voltage (Figure 2.1). A decrease in voltage will correspond to a decrease in sputtering yield, which will decrease the amount of material that is measured on the QCM. At first glance then, the effect of target erosion would be to decrease the required voltage, the sputter yield, and the coating rate.

VII. COATING RATE VS POWER

Before the main experiment was conducted, a side experiment was completed during a calibration run to verify accuracy of the QCM and the automation program. After verification of properly behaved data received by the automation program, I took this opportunity to conduct an experiment to determine the relationship between the gun power output set point and the measured coating rate read from the QCM. Throughout much of the literature on sputter coating, the relevant parameter of the sputter gun power supply was the cathode voltage. Whenever we ran our sputter coaters, however, we would specify the power, allowing the power supply and system to determine the necessary voltage and current. To provide the most relevance to inertial fusion research, I have continued to sputter coat using the constant power mode of the sputter gun power supply. In this way, my data would be readily usable and could be directly compared with existing data. Therefore, in my experiment, I would vary the output power, while monitoring and recording the other parameters, voltage, current, power and coating rate.

For the experiment, I varied the gun power set point to a variety of power levels, ranging from up to 120 Watts down to when the plasma could no longer be sustained (~20 Watts). The sputter target was a partially used (~2000 Watt-hours) and made of copper. Each set point was held constant and averaged for a minute, to average out small scale fluctuations and reduce the noise of the signals. The entire experiment lasted for about 20 minutes, which is short compared to the large scale variation time scale and I do not expect to see any of the long term trends in this data

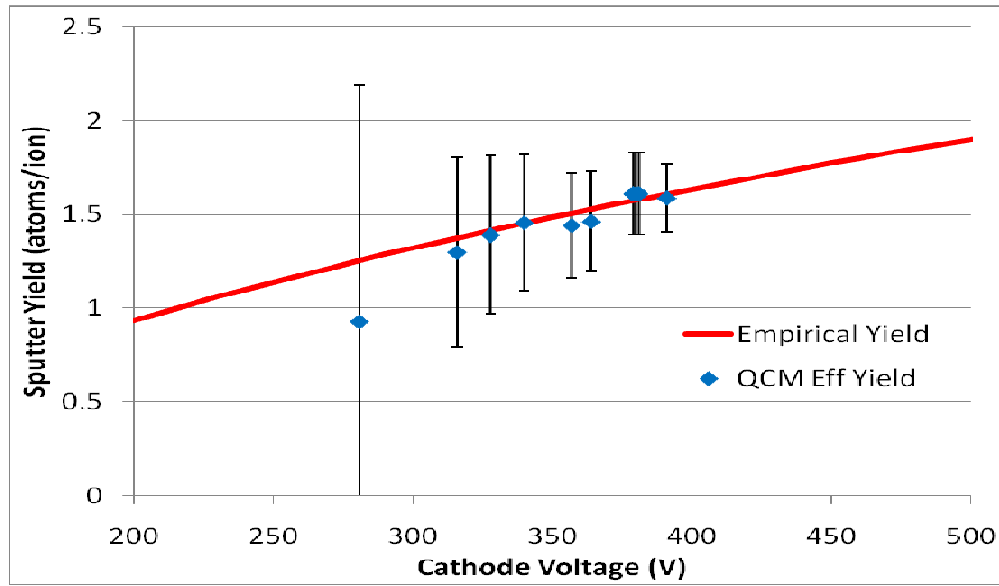


Figure 7.1: Equivalent sputter yield compared to the empirical sputter yield

set. According to the QCM data from the main experiment, I would expect to see a change in coating rate that would be less than 1% from start to finish for the 20 minute experiment. Validation of these data is shown in Figure 7.1, where the equivalent sputter yield is plotted with the empirical sputter yield curve as a function of cathode voltage. I define the equivalent sputter yield as the coating rate measured by the QCM divided by the gun current output, multiplied by a numerical scaling factor. Besides the scaling factor which takes into account the different units and scales involved in the conversion, the physics of the equivalent sputter yield involves an accumulation of material, divided by the rate of ions impacted the surface. It is the apparent sputtering yield, viewed not from the source, but from the detector. The absolute value is arbitrary, but the relative differences between the data points should follow the empirical curve for sputter yield. All of the data points, in the exception of the outlying point with the lowest voltage where the plasma was not sustainable, agree

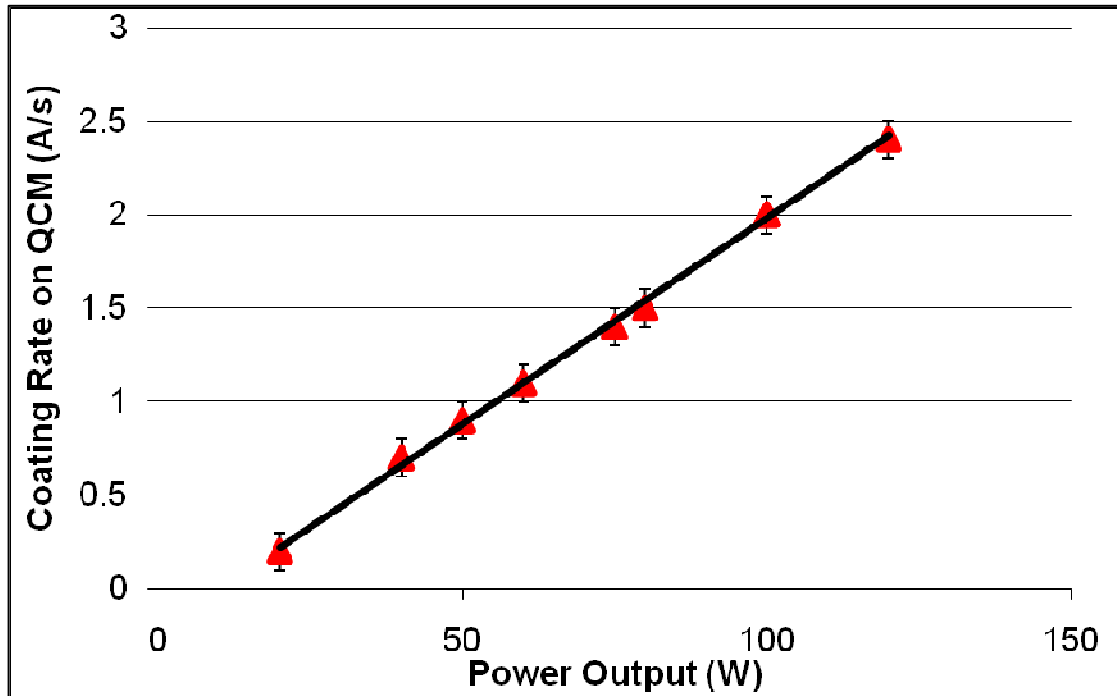


Figure 7.2: Coating rate as a function of gun power set point

very well with the empirical curve. The coating rates as a function of gun power set point are plotted in Figure 7.2, along with a line that corresponds to the best fit. These data would suggest a linear dependence of the coating rate on gun power, neglecting any long term time dependencies which are investigated in the main experiment, which is in agreement with the literature¹⁷. From this experiment over short time scales, the data from my set up is verified by comparing it to previous known results. From this, I have confidence in the validity of my experimental apparatus and measurements.

VIII. CHARACTERIZING THE LIFE OF SPUTTER TARGETS

1. Introduction

The experimental setup described above was used to monitor the coating process as the sputter target erodes. A new sputter target was coated three times for a total of 37 hours at 100 Watts (3700 Watt-hours). At the completion of the experiment, the target was nearly completely eroded and no longer useful for sputtering. For each of the three coating runs, I measured data at four locations: the sputter gun power supply, the copper sputter target, the silicon substrate positioned directly below the target, and the QCM located to the side of the silicon substrate. From this data, the effect of the eroding target on the coating will be shown.

2. Sputter Gun Power Supply

From the recorded sputter gun power supply data, shown in Figure 8.1, the gun output voltage decreases while the current increases in time such that their product results in the constant 100 Watt power output that was the set point. This trend for the current and voltage matches what was found in both the beryllium run data and the preliminary copper data. The trend is much more pronounced with copper than with beryllium, as the percent change for the in voltage copper coater approaches 40%. As the target erodes, the secondary electrons generated as a byproduct of ions impacting the target feel a stronger magnetic field than those that were generated with a new target. This is because the magnetic field strength increases as you get closer to the magnets. These electrons are the ionizing electrons and will be confined closer to the

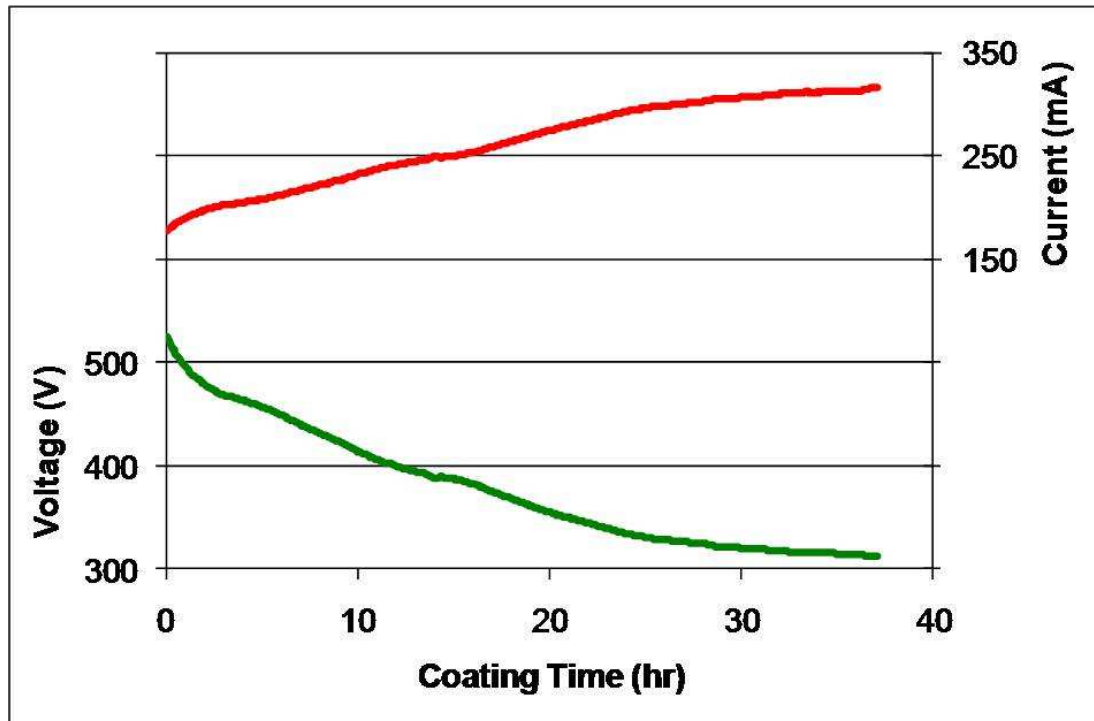


Figure 8.1: Gun power supply data as a function of coating time

target surface, and therefore the ions that are generated will be closer to the target surface. The increase in current that is observed could be the result of a higher argon ion density close to the target in the stronger magnetic field region. The density of argon ions has been shown to increase over a range of increasing magnetic field strength⁹. To maintain the constant power output with the increasing current, the voltage must decrease. The extent to which this will affect the target erosion and coating product will be discussed in the next sections.

3. Copper Sputter Target

By using a single sputter target for the three sequential experiments, the entire life of a target could be examined. By measuring the mass of the target before and

after each run with a scale, the amount of material that was sputtered could be determined. From this measured difference in mass, divided by the run time, the average sputtered mass rate for each run can be calculated and is plotted in Figure 8.2. The average sputtered mass rate decreases in time, indicating that as a target is eroded and develops the race track, less material is sputtered from the target in a given amount of time. This downward trend in time qualitatively follows the decrease in voltage and sputtering rate that were observed previously.

With the mass loss information, we can get an approximate sputter yield as a function of voltage. Dividing the mass loss rate by the molecular mass of copper and the average current for each run (rate of ions incident on the target), we have the sputter yield, which is plotted against the average voltage for each run with the known yield for copper, in Figure 8.3. The calculated sputter yield fits very well to the empirical model. The first data point is the farthest off, and this could be a result of the “burn-in” phase, where a new target shows some irregularity in sputtering. This

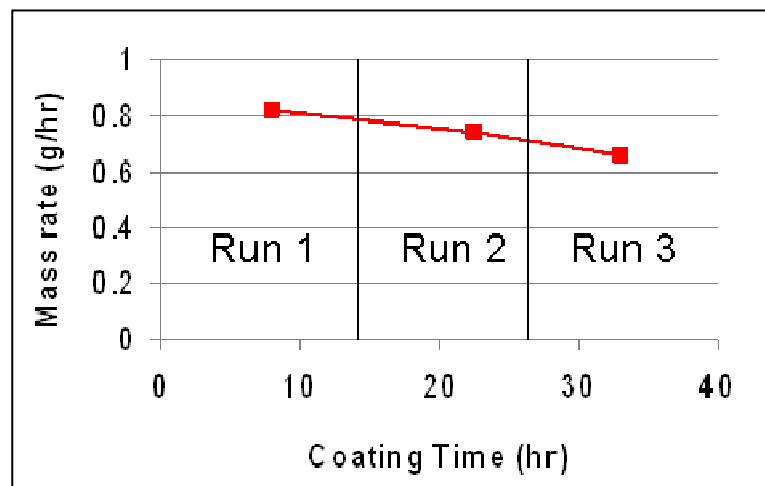


Figure 8.2: Rate of mass sputtered from target as a function of time

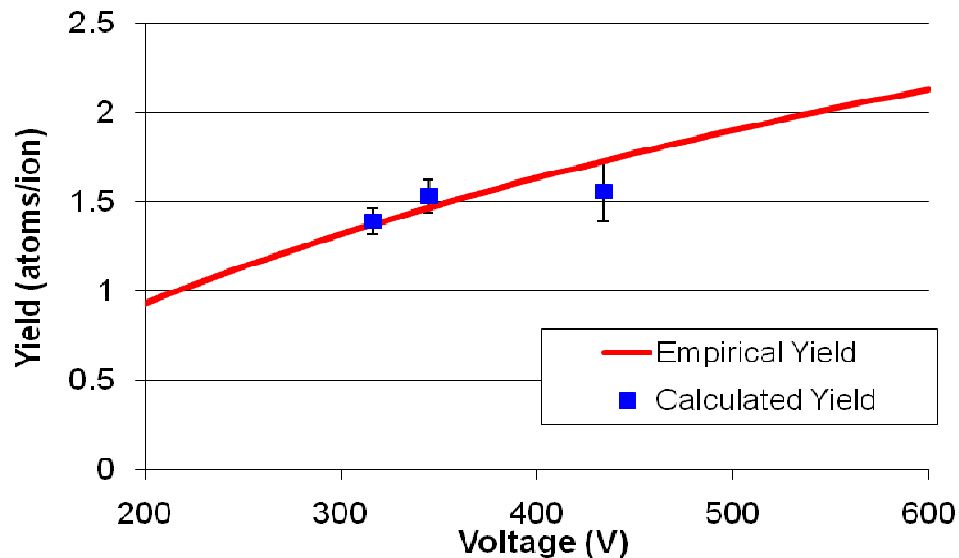


Figure 8.3: Comparison between calculated yield from sputtered mass and empirical copper sputter yield curve

data reinforces the idea that an eroded target will have a decreased sputtering yield and coating rate as a result of a lower voltage, which in turn is the result of the changing geometry and magnetic field strength.

In addition to the mass, I measured the depth profile of the target after each run with a measuring microscope. With the help of digital micrometers, I was able to determine the depth as a function of the position on the target by adjusting the height of the objective lens and recording the height when the image was focused. The initial target had a diameter of 2 inches (~51 mm) and a thickness of about .255 inches (~6.5 mm). Starting from the top of the target and varying the position in only one direction, I measured the depth of the target surface from the initial plane every 1 or 2 mm, noting also the depth and location of the race track. A slight linear variation due to the target not being completely level compared to the objective lens was removed

after the data was recorded. A plot of the surface depth as a function of position and length of time sputtered is shown with the approximate aspect ratio in Figure 8.4. The profile is axially symmetric along the axis perpendicular to and centered in the plane of the target surface. This is shown in Figure 8.5, where the depth profiles are plotted as functions of the radius. I have also included data points from the race track that were measured at different positions on the race track than the scan axis. The normalized depth profiles are plotted in Figure 8.6, where the erosion profile shows self-similarity. These measurements match up to the line scan data and reiterate the symmetry.

Interestingly, very little material has been sputtered from the center and outside edge, while the majority of the sputtered material emanates from the race track which resides at about half of the target radius. Also, from these graphs it can be seen that the maximum depth of the race track is not at a constant radius, but instead slowly moves outward. As seen in Figure 8.7, the location of maximum distance on the magnetic field lines from the target plane, where the field lines are parallel to that plane, also moves out radially as you move toward the target. This agrees with the notion that this is where the majority of ions are located and where the majority of sputtering takes place. In Figure 8.7, you can also see the strength of the magnetic field increasing as you go deeper into the target. Images of target erosion as a function of time sputtered are shown in Figure 8.8.

As a check for consistency between the first two measurement techniques of the target, the mass deficit was compared to the volume deficit from the depth profile,

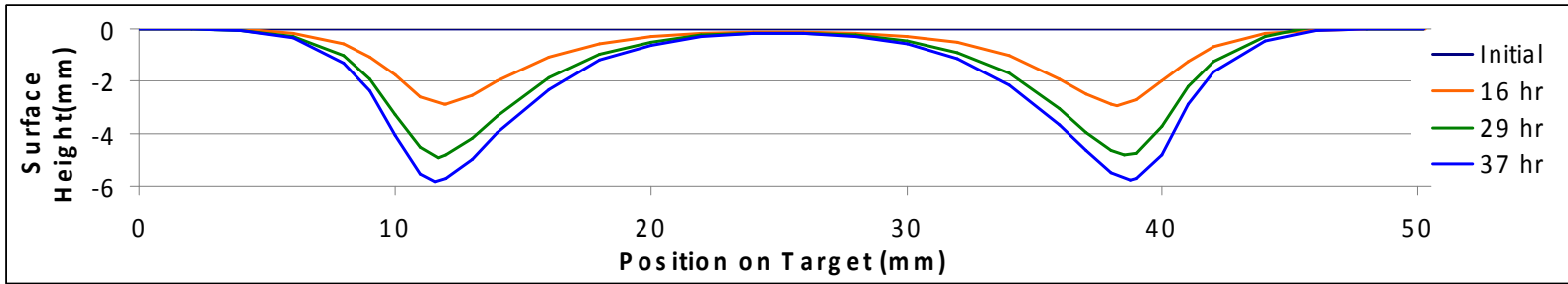


Figure 8.4: Measured depth profile of copper target after each run

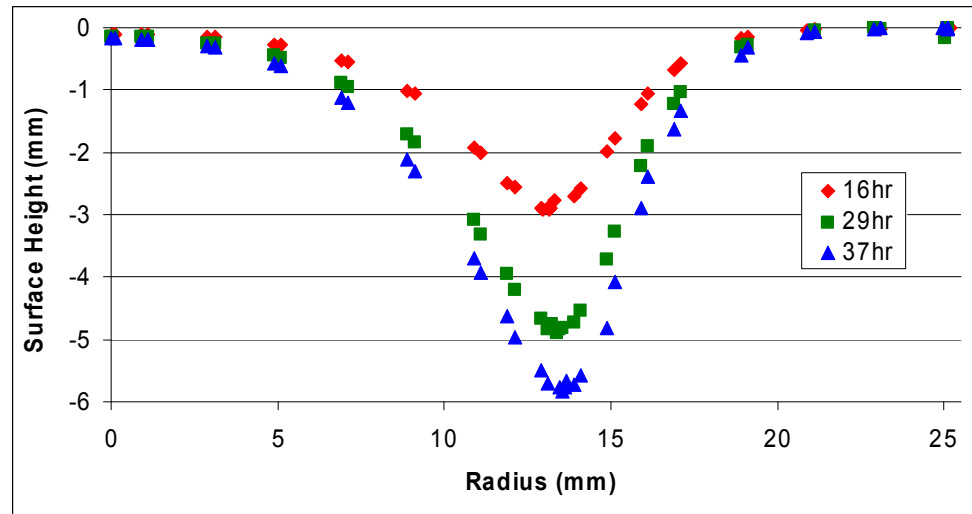


Figure 8.5: Depth profile of copper target as function of the radius

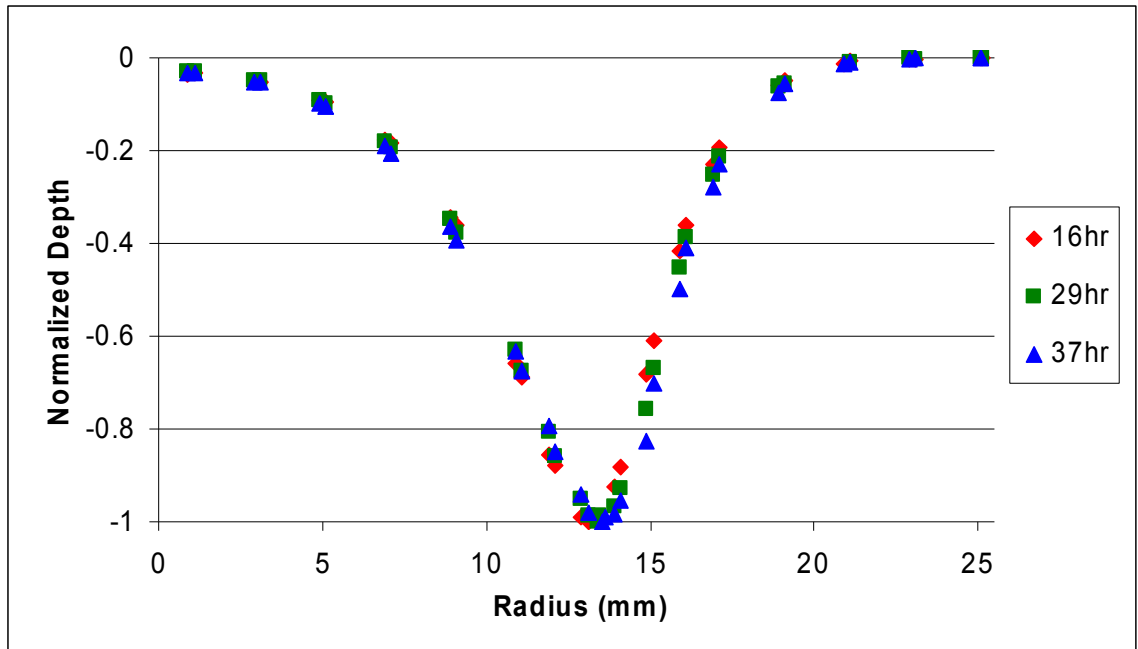


Figure 8.6: Normalized radial race track profiles

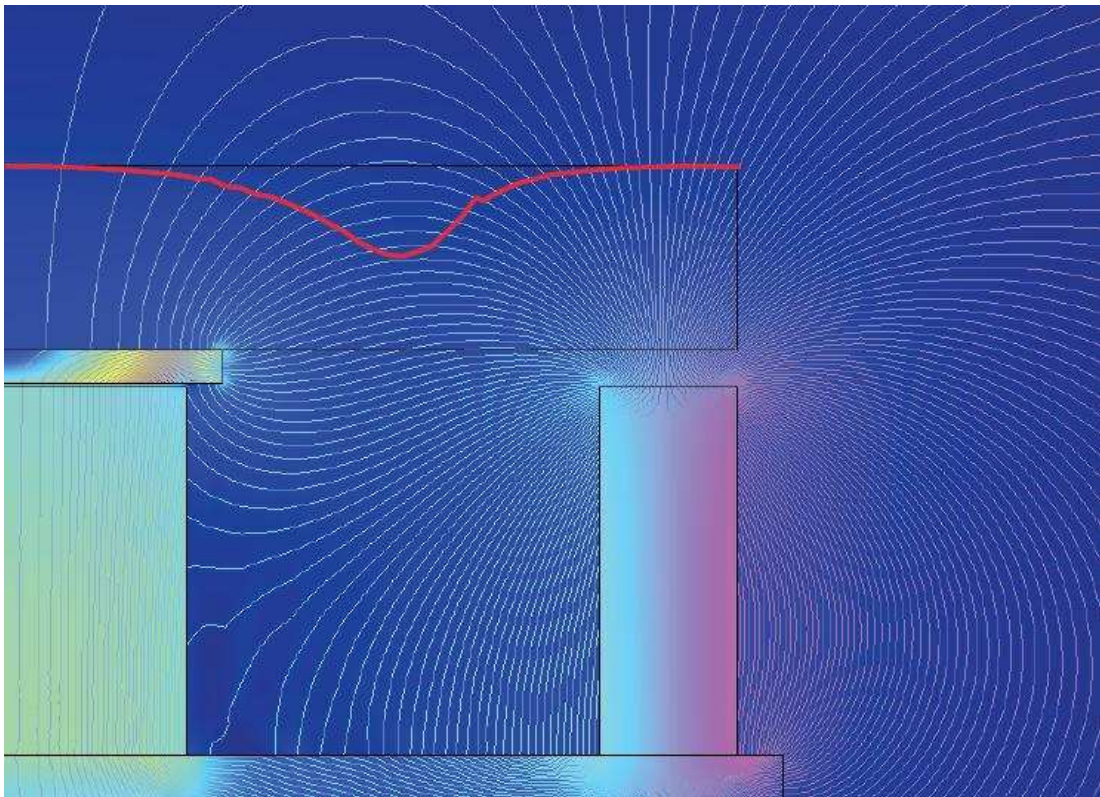


Figure 8.7: Magnetic field lines near the target



Figure 8.8: Comparison of the copper sputter target for different lengths of coating time

multiplied by the density of copper. A first order trapezoidal approximation of the mass sputtered from the depth profile matches the mass deficit with a deviation of at most 1.3%. Thus the depth profile is an accurate representation of the target surface.

After 37 hours of coating at 100 Watts, or 3700 Watt-hours, the race track depth had reached 90% of the initial thickness. I estimate the full life of the target to be around 4000 Watt-hours, which is consistent with a beryllium target running at 25 Watts for a little under a week (~4200 Watt-hours). At this point, the target could no longer be used, because after the plasma erodes completely through the target, it will continue to sputter whatever is behind the target, which can damage the gun and introduce impurities into the coating. While the target is no longer usable as a sputter target, only 24% of the initial target mass has been sputtered. The remaining 76% of target material will either be recycled or discarded.

4. Silicon Substrate

From the silicon substrate placed directly beneath the sputter gun and target, I was able to measure the deposition distribution as a function of position on the substrate. The results from all three runs are plotted in Figure 8.9. Using the stylus probe, I scanned along both the x and y axes at quarter inch intervals, see Figure 4.1. The data from each axis is similar, again showing the symmetry of the coating. The distribution of the coated material across the wafer can be described with the previously discussed $\cos^4(\theta)$ fit, where θ is the angle measured between the line normal to the target and the line connecting the sputtering source (target) to the

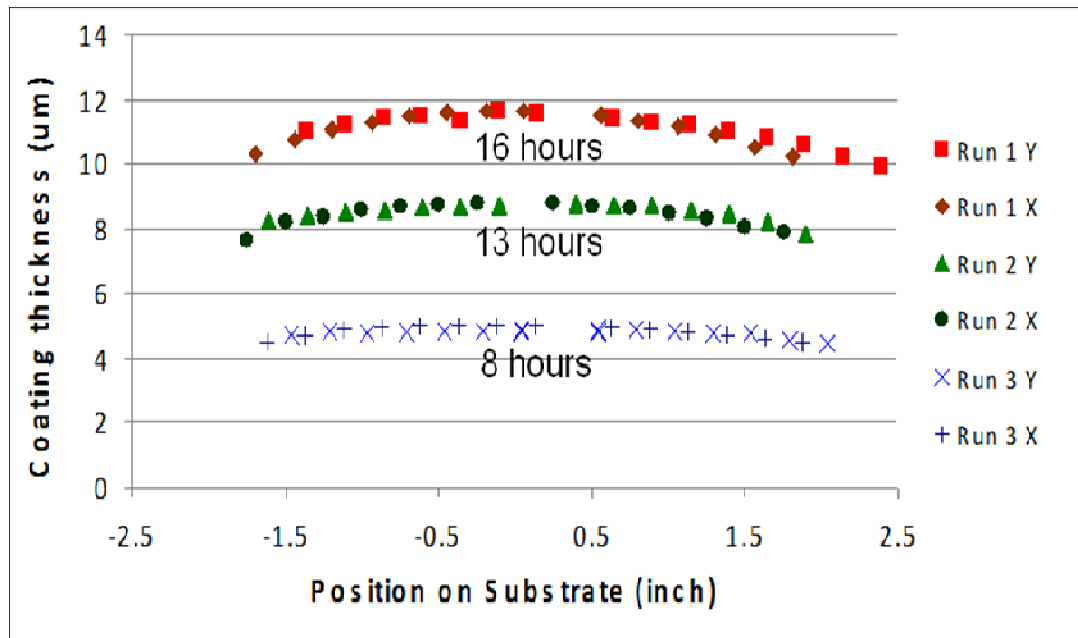


Figure 8.9: Copper thickness on silicon substrate from both axes

location on the substrate. The coated thicknesses are plotted with their corresponding cosine⁴ fit curves, in Figure 8.10. The coating rate between the first and last run decreases by about 15 %. It is important to note that this dependence is consistent for all three coating runs, indicating a uniformity local to the four inch wafer directly under the target (or similarly when θ less than or equal to about 15°). Despite the erosion of the target and decreasing sputter yield and coating rate, the substrate shows spatial uniformity directly below the target, that is independent of the coating time.

5. Quartz Crystal Microbalance

In addition to the silicon wafer, the QCM recorded the thickness of deposited material from the sputtering process. The QCM has the additional benefit that it provides the thickness and coating rate during the run, when the substrate cannot be

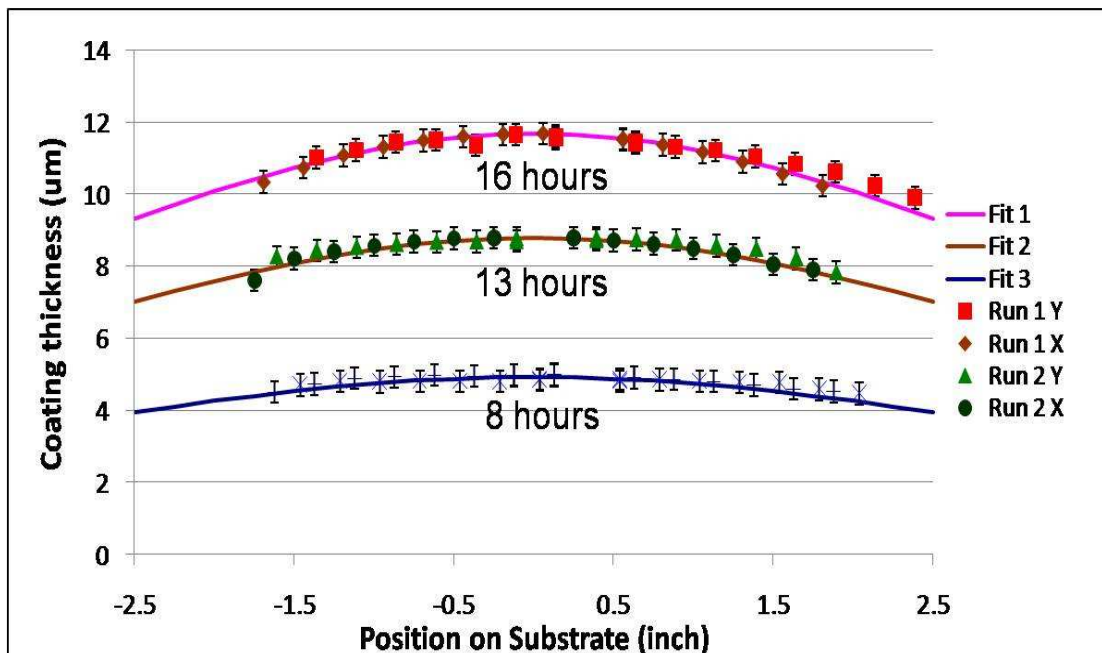


Figure 8.10: Thickness on silicon substrate with \cos^4 fit

accessed. Compared to the silicon wafer, the QCM measurements were within 7.5 % and showed similar trends. After applying a $\cos^3(\theta) * z_{\text{substrate}}^2 / z_{\text{QCM}}^2$ factor to the QCM data due to the geometry of the QCM's location, the difference between the silicon substrate and the QCM goes down to about 3% for the first run and 5% for the third run. A graph of the coating rates of each run stitched together is plotted in Figure 8.11. The coating rate increases during an initial period of about eight hours, but then decreases by more than 20% over the remaining 29 hours. This initial period could be the “burn-in” phase previously discussed. These results are similar to those from the silicon substrates and bring further consistency to the data.

The instantaneous effective sputter yield from the QCM data is plotted as a function of cathode voltage in Figure 8.12. Here we can see the trend of the sputter yield as seen by the QCM as the target erodes. These data indicate a deviation from

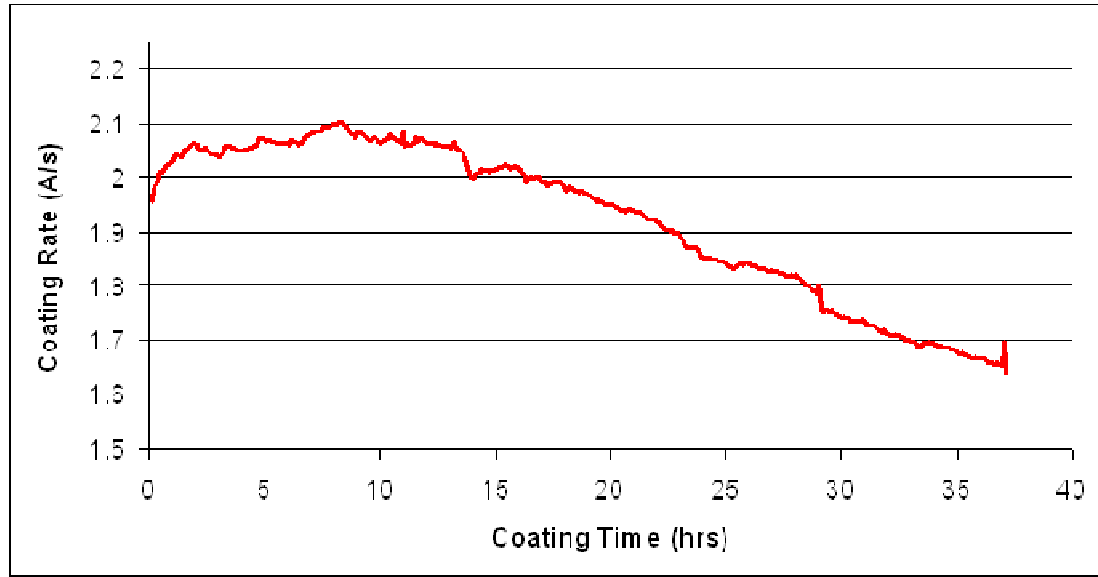


Figure 8.11: Copper coating rate as measured by the QCM

the empirical curve such that the sputtering yield for an eroding target decreases in time faster than from the voltage dependence alone. Here is a clear indication of a long time scale variation as a result of target erosion.

6. Summary of Results

If we normalize the coating rate from the QCM, the thickness deposition rate on the center line of the silicon wafer, and the mass rate of loss by the target by their values after the first run, we have a normalized sputter rate that varies by run and location of the measurement. This is plotted in Figure 8.13. At each measurement location, the sputter rate decreases in time. This is consistent with the data analyzed so far. The QCM and silicon wafer have a similar trend, but the QCM decreases slightly faster. This can be explained geometrically, as the QCM is away from the centerline, where any angular dependence would be stronger.

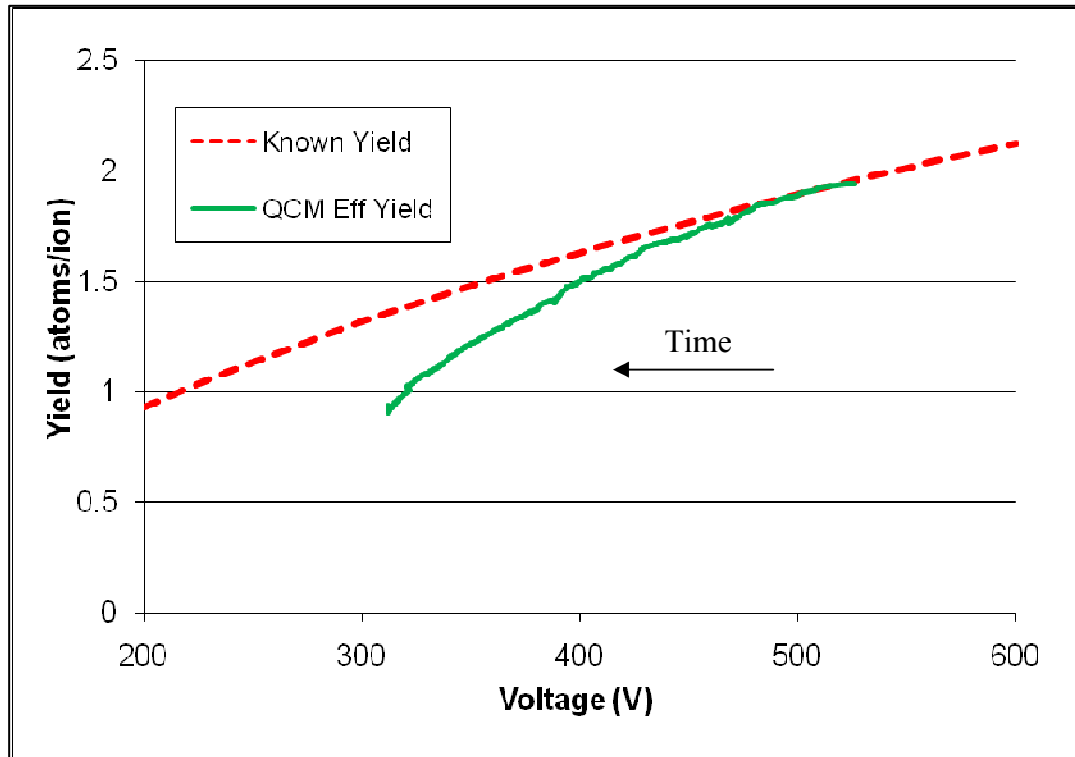


Figure 8.12: Comparison of QCM equivalent and empirical sputter yields

The normalized mass rate, however, decreases much faster than the other two. This is a strange result. Basically, the sputter rate from the sputter target is decreasing faster than deposition rate on the substrates. Owing to the fact that material cannot be spontaneously created at the substrate, the spread of material from the sputter target must be narrowing or focusing the material along the centerline axis. The proportion of material that for a new target would have gone to the chamber walls is now being focused toward the substrate. Referring back to the cosine distribution of sputtered atoms from a point source, if we assume the source of sputtering is located at the bottom of the race track, then part of that distribution will be blocked by the surface of the target. A simple representation of this is shown in Figure 8.14.

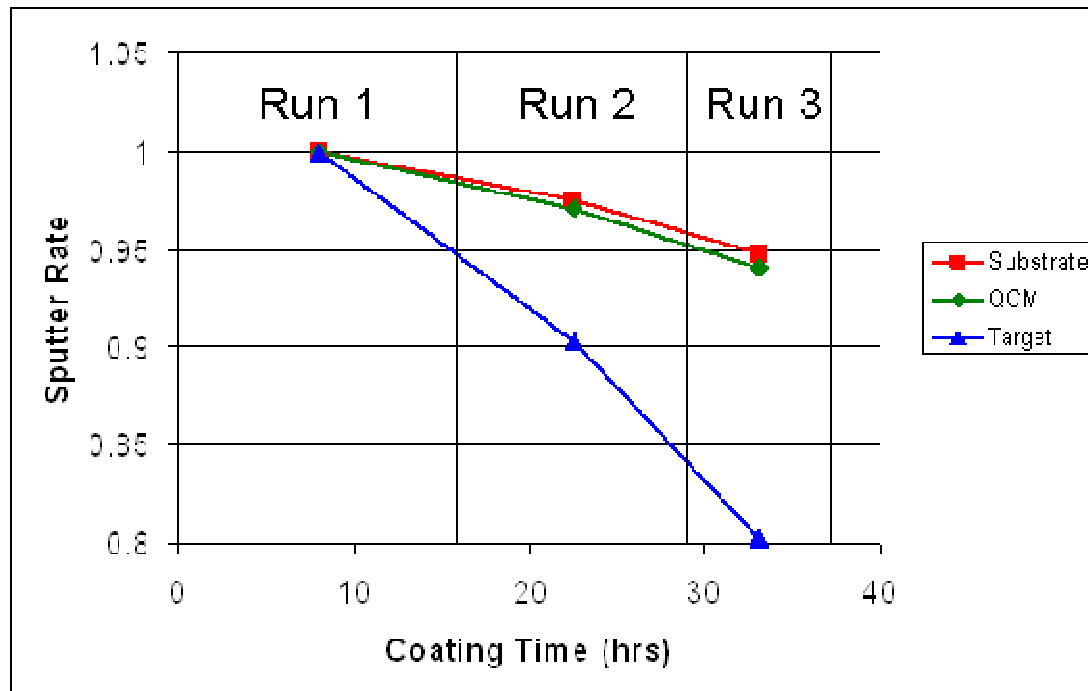


Figure 8.13: Normalized coating rates

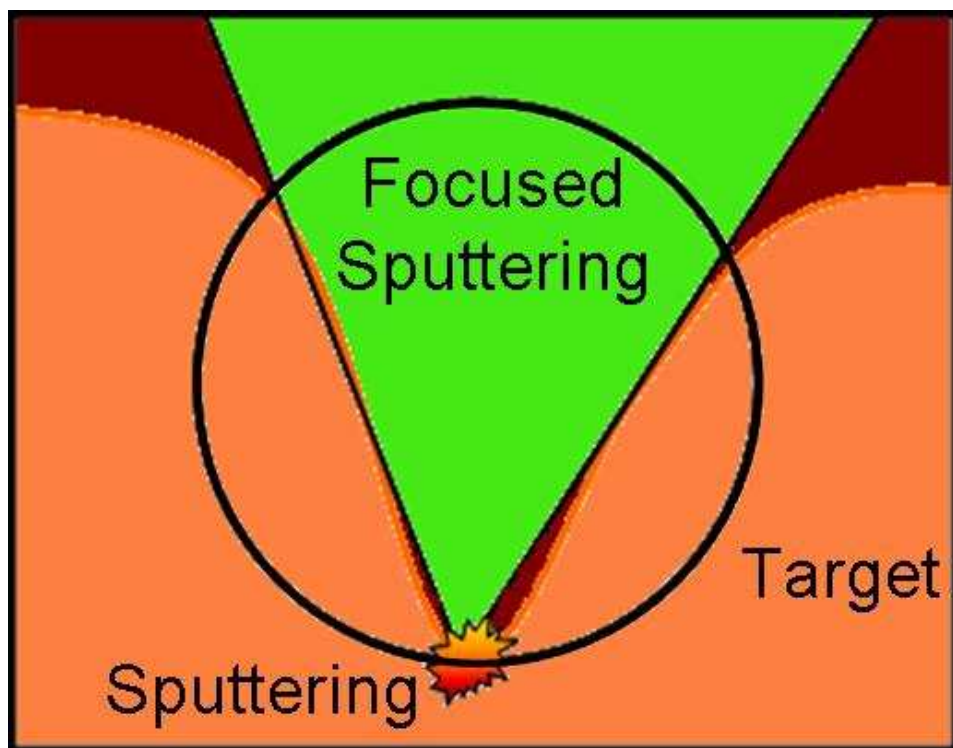


Figure 8.14: Diagram of focusing effect of race track on sputtered material

The interaction of sputtered material with the target can result in several things. The copper atoms can be reflected by means of an elastic collision, and the resulting sputtering distribution will be focused. Another possibility is that the copper will stick the target surface, with a possibility of resputtering. Either or both of these possible scenarios would have the effect of focusing the sputtered material toward the substrate, which is good news for sputtering applications, as it suggests more efficient use of the sputter target as it erodes. This would be an interesting topic for further experimentation or numerical simulation.

IX. CONCLUSION

When coating with a dc magnetron sputter coater, determining the time variation of the coating depends on the time scale and power used. Initially, there is a “burn-in” phase, where the coating rate increases in time. For coatings of 100 Watt-hours or less, it is shown that the sputter yield follows the empirical curve very well and the coating rate is linearly proportional to the power output of the sputter gun power supply. For longer coatings, especially when they last the life of the target (~4000 Watt-hours), the sputtering yield and coating rate as measured from the substrate, decrease by about 15%. The amount of sputtering decreases faster than the coating rate at the substrate because the sputtered material is focused by the walls of the target.

It would seem that there are two effects from target erosion and race track growth on the amount of material received at the substrate. The first effect is a decrease in coating rate that occurs everywhere. Directly below the target, the coating rate was reduced 16%, but followed a $\cos^4(\theta)$ distribution. The sputtered mass rate decreases by about 20% and the sputtering yield drops 10%. This is due to the decreasing gun voltage (~40%), but this in turn is caused by the changing geometry of the target and strength of the felt magnetic field. The second effect is spatially dependent and results from a focusing of sputtered material that reduces the amount of material that reaches the substrate locations with a large angle θ . For my coater configuration, the QCM showed a 20% decrease in coating rate. These values are geometry dependent, but they do show that the most uniform coating will be achieved

directly below the center of the target, again varying up to 16% during the life of the target.

Another result from these data confirms that target utilization is very poor. From the initial target mass, less than one quarter is actually sputtered, and only a fraction of that is actually retained as a useful coating. This is a source of significant waste, and can be quite costly for more expensive materials such as gold or platinum. As is shown on the measured depth profile of the eroded target, very little material is sputtered from the center or edges of the target. A more efficiently manufactured target might contain a cheaper material, like copper, molded in the shape of a used target, with the remaining volume filled with the more expensive material, i.e. gold. The depth profile is liable to change for each sputter gun and corresponding magnetic field, but with a generous margin it would not be unreasonable to make two targets with the equivalent of one full target of expensive material. This could save money in fabrication and lower the price for industry. For more expensive materials, it may be worth looking into. Another option to increase target utilization is incorporating a ferromagnetic backing plate or mold that would manipulate the magnetic fields to use more of the target²³.

From these experiments, it is evident that the sputter coating process does change in time. The mass depletion rate, the coating rate directly below the target and the coating rate measured by the QCM away from the center line all decreased as the target eroded. The mass depletion rate decreased much faster, however, implying that the distribution of sputtered material is narrower in the case of the eroded target, than

for the new target. At the location directly beneath the sputter target, which is of the most interest to our application, the change in coating rate decreases to about 16% of the initial rate. This effect is more pronounced as the angle θ is increased and will introduce thickness variations if coating a large area (large θ). The decrease in rate can be compensated with an increased run time; however, the effect of the slower deposition rate on the quality of the coating is not clear.

Further experiments would be useful in exploring these time-dependent variations, such as the proposed focusing effect. Future experiments would investigate a varying substrate distance to provide a more complete understanding of the coated thickness distribution, as well as other quantitative coating measurements.

For those that work on simulating the sputter coating process, this data will be very helpful. Experimental conditions of time-varying power supply data and erosion profiles will help in the simulation of short and long time coating simulation.

This was not intended to be an exhaustive study, but an attempt to understand the trends of the time varying process. The results of these experiments could be applied to many sputtering applications. Coating thicknesses can be more accurately estimated, even without a QCM, from the gun power set point and the erosion of the target. These results do suggest future topics of research and numerical study, such as the mechanism of erosion of the target or creating a model to simulate the narrowing of the distribution and the shadowing. With this data, we move one step closer to the goal of being able to repeatedly mass produce the perfect shell for Inertial Confinement Fusion.

APPENDIX

On the following pages are screen dumps of the LabVIEW programs that I created for automation, process monitoring, and data recording. The full automation program for the beryllium sputter coater incorporated 37 different subvis and is about 1.92 MB. There was one main window from which all tasks could be accessed. While coating, there are two active windows, data display and process control. The following figures show the front panels and block diagrams of the vi and main subvis.

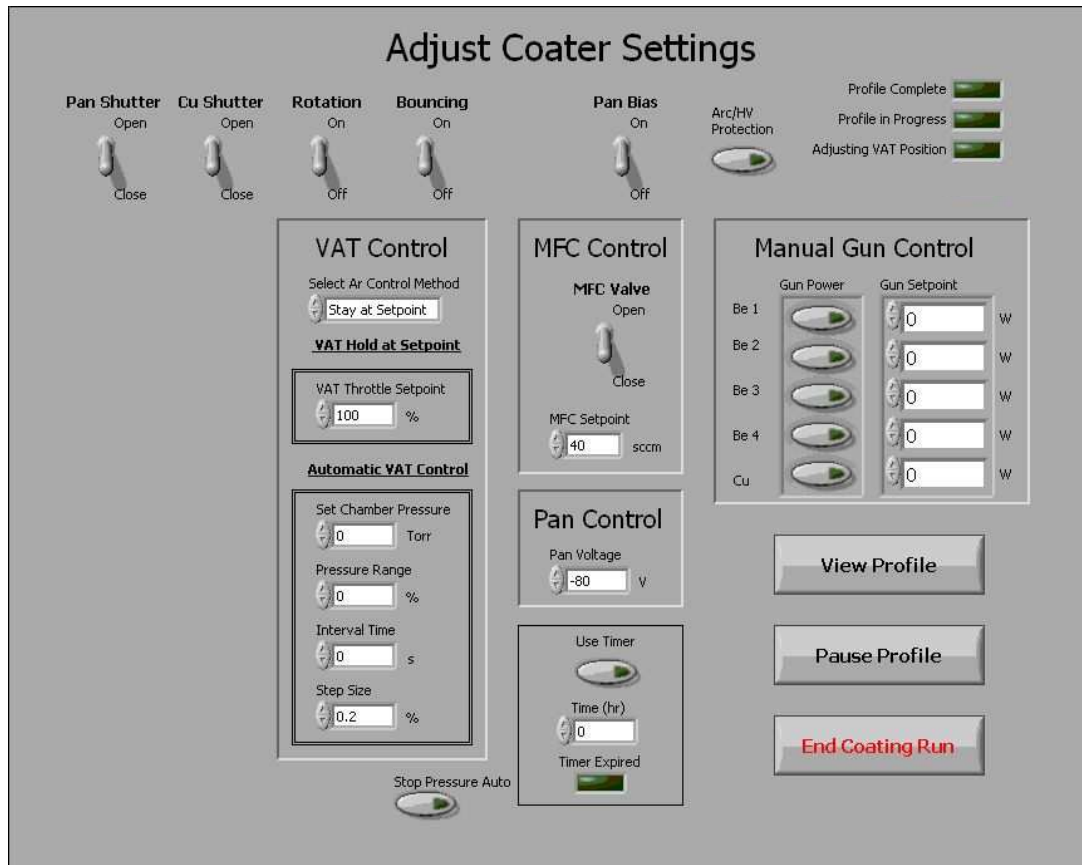


Figure 10.1: Adjust Coater Settings subvi front panel

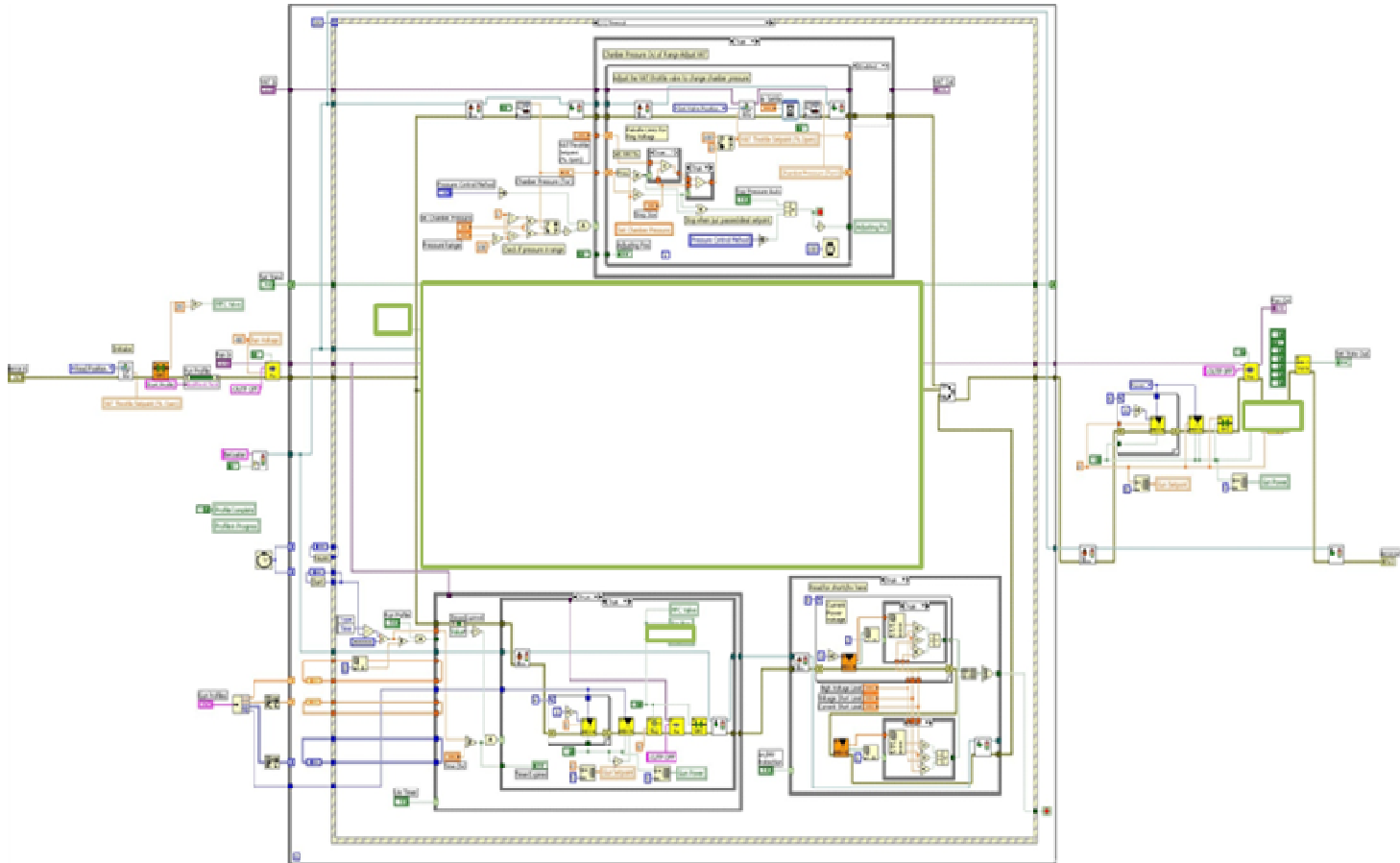


Figure 10.2: Adjust Coater Settings subvi block diagram

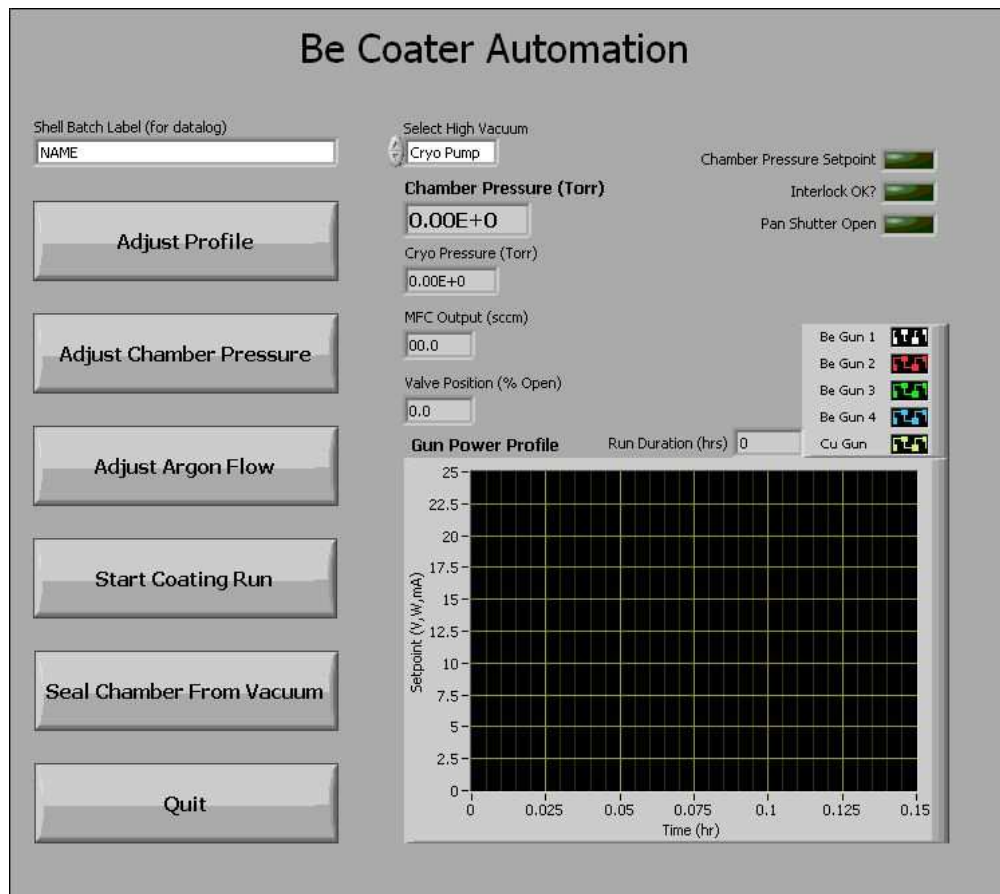


Figure 10.3: Be Coater Main vi front panel

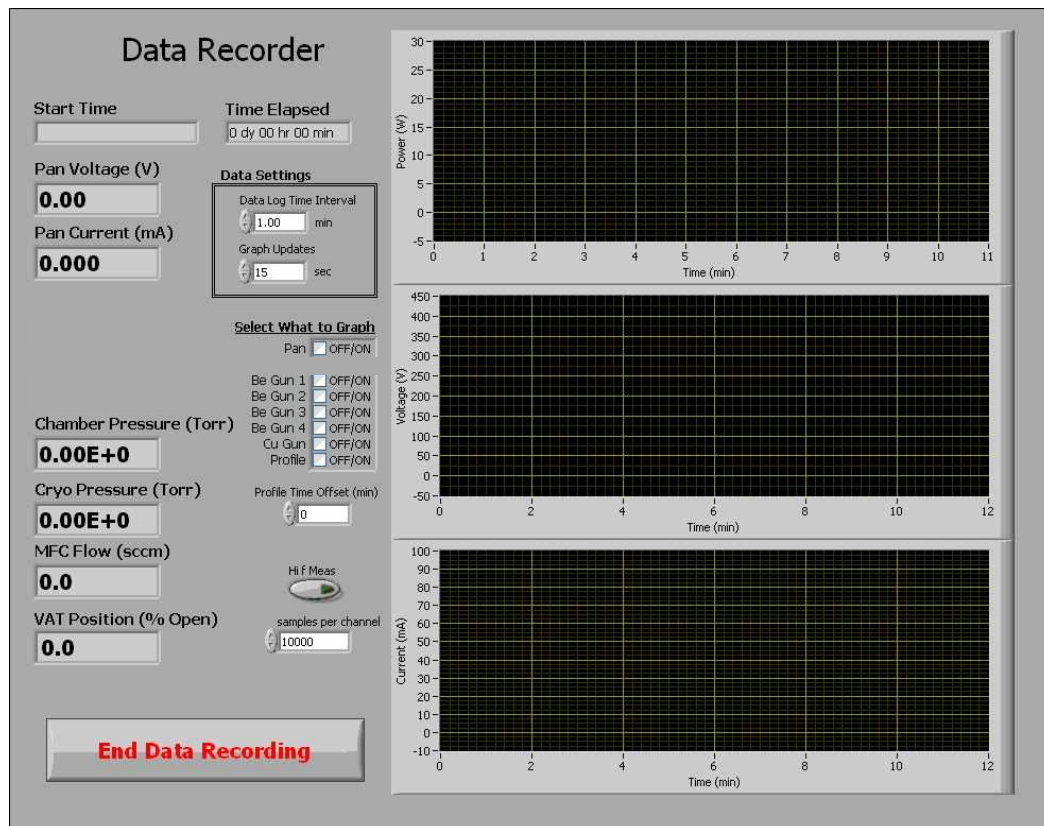


Figure 10.4: Data Recorder subvi front panel

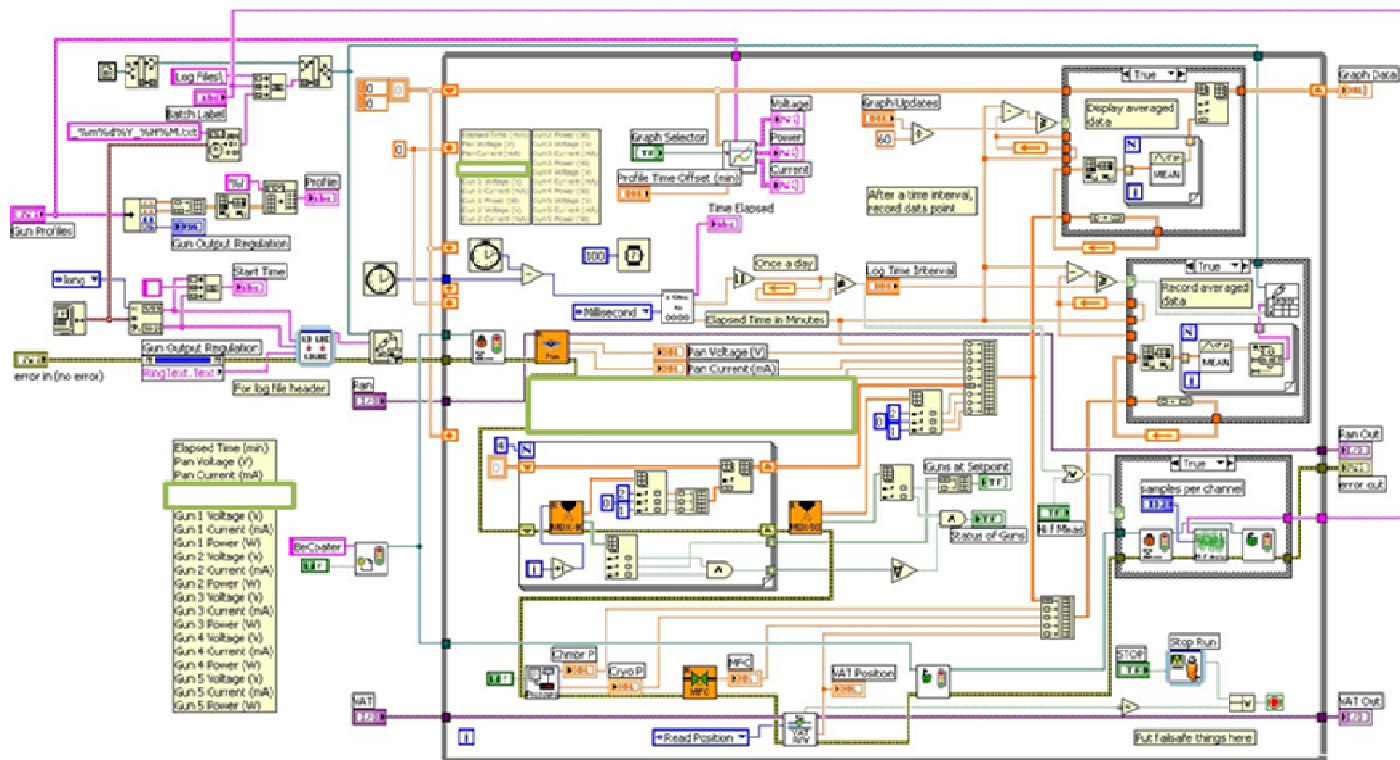


Figure 10.5: Data Recorder subvi block diagram

The second automation program that I created involved three coaters, one of which housed the copper experiments from this thesis. This program did not need to control as much as the beryllium coater. The program consists of 14 subvis and is 691 kB. This program was designed to be continuously running with minimal impact on the computer performance. It would automatically detect if a sputter gun was activated and begin recording data. This program is meant to gather data in the background, while also having the option of remotely turning off the coater(s) at a preset time or thickness (measured by the QCM). The following figures show the front panel and block diagram of the main program vi.

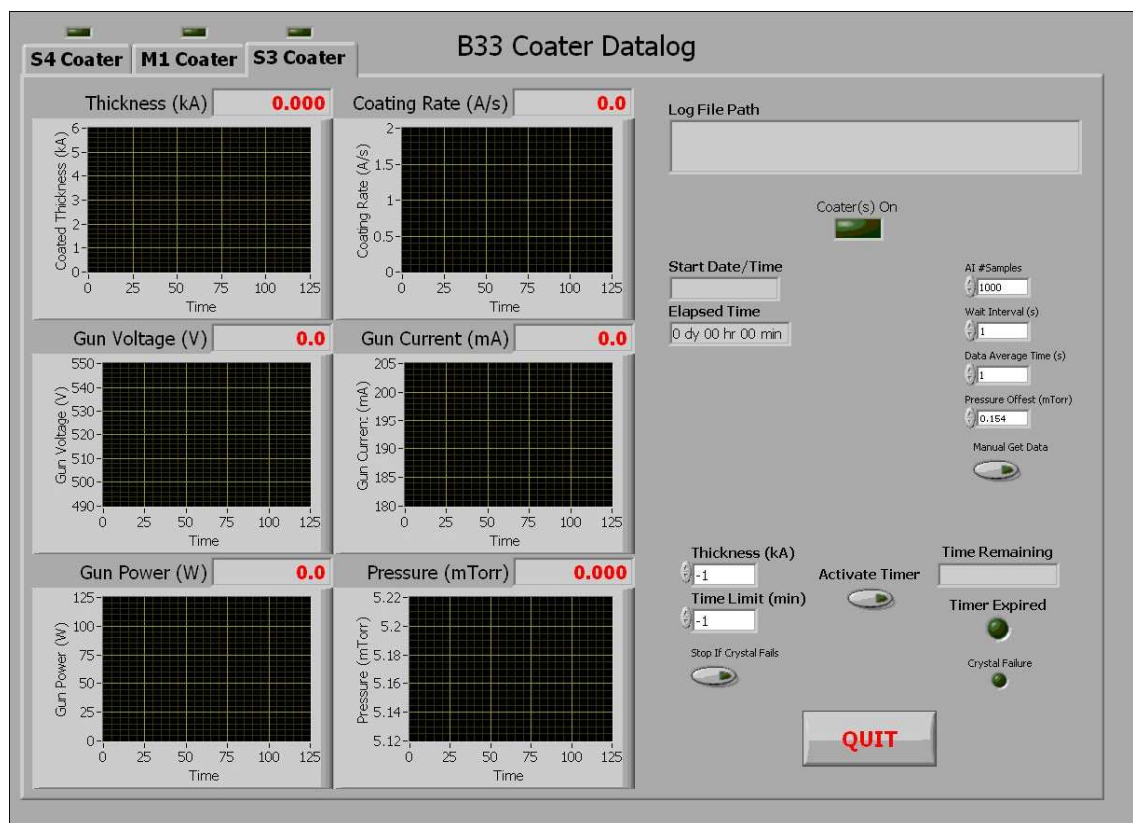


Figure 10.6: Multiple Coater Datalog vi front panel

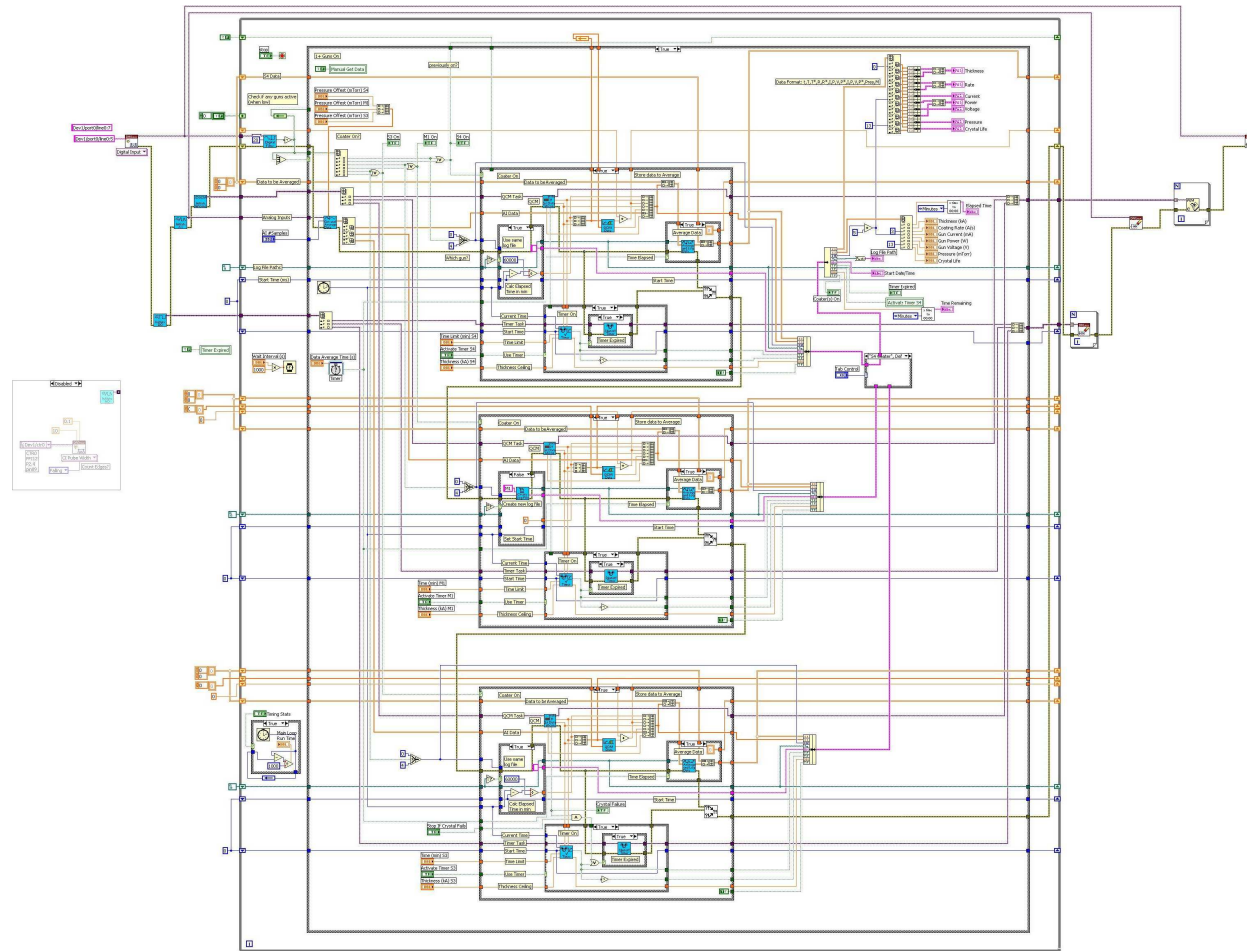


Figure 10.7: Multiple Coater Datalog vi block diagram

REFERENCES

1. Institut für Allgemeine Physik, Technische Universität Wien. “A Simple Sputter Yield Calculator.” 2009.
<<http://www.iap.tuwien.ac.at/www/surface/sputteryield>>
2. J. Bordes, C. Bordes, E. Ehret, R. Gschwind, and P. Bauer. “Theoretical sputtering yields of Al and Mg targets in physical vapor deposition processes.” *J. Vac. Sci. Technol. A* 19 (2001) pp. 805-811.
3. M. Bloomfield and T. Cale. “Modeling of Ionized Magnetron Sputtering of Copper.” *Mat. Res. Soc. Symp. Proc.* 616 (2000) pp.147-152.
4. Rainer Behrisch and Wolfgang Eckstein. *Sputtering by Particle Bombardment*. Springer, Berlin (2007).
5. Michael A. Lieberman and Allan J. Lichtenberg. *Principles of Plasma Discharges and Materials Processing*. Wiley, New York (2005).
6. Qiu Q, Li Q, Su J, Jiao Y, and Finley J. “Simulation to Predict Target Erosion of Planar DC Magnetron.” *Plasma Science and Technology* 10 (2008) pp. 581-587.
7. E. Bultinck, I. Kolev, A. Bogaerts, and D. Depla. “The importance of an external circuit in a particle-in-cell/Monte Carlo collisions model for a direct current planar magnetron.” *Journal of Applied Physics* 103 (2008) pp. 1-9.
8. Haibo Huang. *Pictures of Plasma and Magnetic Field Measurements*. General Atomics. 2008.
9. E. Bultinck and A. Bogaerts. “The effect of the magnetic field strength on the sheath region of a dc magnetron discharge.” *J. Phys. D: Appl. Phys.* 41 (2008) pp. 1-5.
10. U. Helmersson, M. Lättemann, J. Bohlmark, A. Ehasarian, and J. Gudmundsson. “Review Ionized physical vapor deposition (IPVD): A review of technology and applications.” *Thin Solid Films* 513 (2006) pp. 1-24.
11. I. Kolev and A. Bogaerts. “Detailed Numerical investigation of a DC Sputter Magnetron.” *IEEE Transactions on Plasma Science* 34 (2006) pp. 886-894.
12. S. Ueda, T. Ohsaka, and S. Kuwajima. “Molecular dynamics evaluation of self-sputtering beryllium.” *Journal of Nuclear Materials* 258-263 (1998) pp. 713-718.

13. E. Shidoji, M. Nemoto, T. Nomura, and Y. Yoshikawa. "Three-Dimensional Simulation of Target Erosion in DC Magnetron Sputtering." *Jpn. J. Appl. Phys.* 33 (1994) pp. 4281-4284.
14. E. Shidoji, H. Ohtake, N. Nakano and T. Makabe. "Two-Dimensional Self-Consistent Simulation of a DC Magnetron Discharge." *Jpn. J. Appl. Phys.* 38 (1999) pp. 2131-2136.
15. Q. Qiu, Q. Li, J. Su, Y. Jiao and J. Finley. "Influence of Operating Parameters on Target Erosion of Rectangular Planar DC Magnetron." *IEEE Transactions on Plasma Science.* 36 (2008) pp. 1899-1906.
16. I. Kolev and A. Bogaerts. "Numerical study of the sputtering in a dc magnetron." *J. Vac. Sci. Technol. A* 27 (2009) pp. 20-28.
17. I. Knittel, M. Gothe, and U. Hartmann. "Quantitative analysis of sputter processes in a small magnetron system." *J. Vac. Sci. Technol. A* 23 (2005) pp. 1714-1720.
18. G.H. Rue and H.K. Kim. "A two-inch dc/rf circular magnetron sputtering gun for a miniature chamber for an *in situ* experiment." *Review of Scientific Instrument.* 69-4 (1998) pp. 1616-1621.
19. R. Kolasinski, J. Polk, D. Goebel, and L. Johnson. "Carbon sputtering yield measurements at grazing incidence." *Applied Surface Science* 254 (2008) pp. 2506-2515.
20. T. Yagisawa and T. Makabe. "Modeling of dc magnetron plasma for sputtering: Transport of sputtered copper atoms." *J. Vac. Sci. Technol. A* 24 (2006) pp. 908-913.
21. P. C. Zalm. "Quantitative Sputtering." *Surface and Interface Analysis* 11 (1988) pp. 1-24.
22. U. Kwon and W. Lee. "Multiscale Monte Carlo Simulation of Circular DC Magnetron Sputtering: Influence of Magnetron Design on Target Erosion and Film Deposition." *Japanese Journal of Applied Physics* 45 (2006) pp. 8629-8638.
23. C. Nouvellon, P. Lefèvre, J.P. Dauchot, R. Papantonio and M. Hecq. "Target Utilization Improvement by Pole Pieces Insertion in a Magnetron Sputtering Target." *Plasma Process. Polym.* 2007 pp. S637-S639.